Published in final edited form as:

Cell Rep. 2018 November 13; 25(7): 1786–1799.e4. doi:10.1016/j.celrep.2018.10.058.

Human COX7A2L Regulates Complex III Biogenesis and Promotes Supercomplex Organization Remodeling without Affecting Mitochondrial Bioenergetics

Teresa Lobo-Jarne[1,6], **Eva Nývltová**[2,6], **Rafael Pérez-Pérez**[1], **Alba Timón-Gómez**[2], **Thibaut Molinié**[3], **Austin Choi**[2], **Arnaud Mourier**[3], **Flavia Fontanesi**[4], **Cristina Ugalde**[1,5,*], and **Antoni Barrientos**[2,4,7,*]

[1]Instituto de Investigación Hospital 12 de Octubre (i+12), 28041 Madrid, Spain

[2]Department of Neurology, University of Miami Miller School of Medicine, Miami, FL 33136, USA

[3]Université de Bordeaux and Centre National de la Recherche Scientifique, Institut de Biochimie et Génétique Cellulaires UMR 5095, Bordeaux, France

[4]Department of Biochemistry and Molecular Biology, University of Miami Miller School of Medicine, Miami, FL 33136, USA

[5]Centro de Investigación Biomédica en Red de Enfermedades Raras (CIBERER), U723, 28029 Madrid, Spain

[6]These authors contributed equally

[7]Lead Contact

SUMMARY

The mitochondrial respiratory chain is organized in a dynamic set of supercomplexes (SCs). The COX7A2L protein is essential for mammalian SC III_2+IV assembly. However, its function in respirasome (SCs I+III_2+IV_n) biogenesis remains controversial. To unambiguously determine the COX7A2L role, we generated *COX7A2L*-knockout (*COX7A2L*-KO) HEK293T and U87 cells. *COX7A2L*-KO cells lack SC III_2+IV but have enhanced complex III steady-state levels, activity, and assembly rate, normal *de novo* complex IV biogenesis, and delayed respirasome formation. Nonetheless, the KOs have normal respire some steady-state levels, and only larger structures (SCs $I_{1–2}$+III_2+IV_{2-n} or megacomplexes) were undetected. Functional substrate-driven competition assays showed normal mitochondrial respiration in *COX7A2L*-KO cells in standard and nutritional-, environmental-, and oxidative-stress-challenging conditions. We conclude that

*Correspondence: cugalde@h12o.es (C.U.), abarrientos@med.miami.edu (A.B.).

AUTHOR CONTRIBUTIONS

F.F., C.U., and A.B. designed the study. T.L.-J. and F.F. created and characterized the HEK293T *COX7A2L*-KO line. E.N. created the U87 *COX7A2L*-KO line and characterized the two KO lines. R.P.-P. performed doxycycline experiments and contributed to the characterization of KO cell lines. A.T.-G. developed oxidative stress and protein import assays. A.C. performed heat shock assays. T.M. optimized methods for high-resolution oxygraphy, and T.M. and A.M. performed OXPHOS measurements. T.L.-J., C.U., and A.B. wrote the paper, and all authors read and edited the manuscript.

DECLARATION OF INTERESTS

The authors declare no competing interests.

COX7A2L establishes a regulatory checkpoint for the biogenesis of $CIII_2$ and specific SCs, but the COX7A2L-dependent MRC remodeling is essential neither to maintain mitochondrial bioenergetics nor to cope with acute cellular stresses.

Graphical Abstract

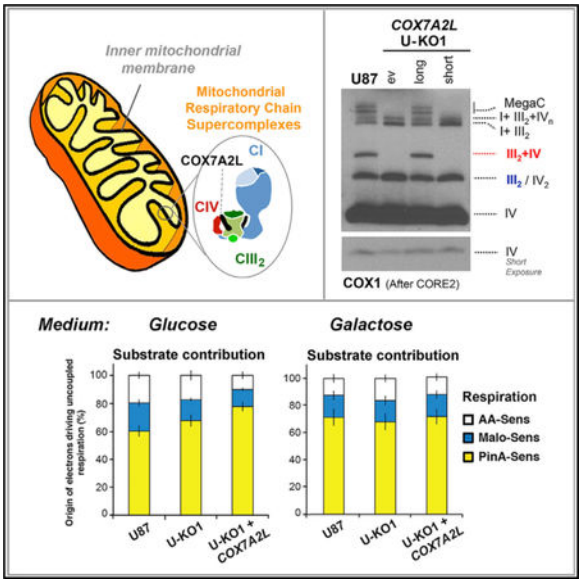

In Brief

The role of COX7A2L in mitochondrial respiratory chain supercomplex biogenesis and function remains controversial. By analyzing COX7A2L- knockout human cells, Lobo-Jarne et al. report that this protein promotes specific respiratory chain complex assembly and organization remodeling but does not affect mitochondrial bioenergetics in physiological, nutritional, or oxidative stress conditions.

INTRODUCTION

The mitochondrial respiratory chain (MRC) consists of four enzymatic multimeric complexes (CI to CIV) and two mobile electron carriers (coenzyme Q and cytochrome *c*), which catalyze electron transfer from reducing equivalents (NADH and $FADH_2$) to molecular oxygen. The process is coupled to the generation of a proton gradient that drives ATP synthesis by the ATP synthase through oxidative phosphorylation (OXPHOS). The proton-pumping complexes (CI, CIII, and CIV) can assemble into higher supramolecular structures known as supercomplexes (SCs) (Cruciat et al., 2000; Schägger and Pfeiffer, 2000). Mammalian CI is primarily found assembled in SCs, either interacting with the CIII dimer ($CIII_2$) to form SC $I+III_2$, or with both $CIII_2$ and CIV to form SC $I+III_2+IV_1$, to which additional CIV monomers can be added. These structures are known as the respirasomes (Schägger and Pfeiffer, 2000), since they were initially proposed to contain all the components required to transfer electrons from NADH to molecular oxygen (Ac´ın-Pérez et al., 2008). In addition, $CIII_2$ and CIV form the scarce SC III_2+IV that coexists with the relatively abundant SCs $I+III_2+IV_{0–4}$, as well as with $CIII_2$, CIV_2, and monomeric CIV

(Lobo-Jarne and Ugalde, 2018). The structural and functional organization of the MRC complexes is currently considered to be dynamic, where the proportion of free complexes and SCs is possibly modulated to adapt ATP production to changing cellular metabolic demands and environmental conditions (Acin-Perez and Enriquez, 2014). However, the functional roles of the SCs remain intriguing. The general arrangement of the MRC in SCs was initially suggested to confer catalytic advantages to the system, as it was proposed to enhance the electron flux through substrate channeling (Bian-chi et al., 2004), and to allow optimization of the available metabolic substrates via partitioned coenzyme Q and cytochrome *c* pools (Lapuente-Brun et al., 2013). However, direct spectroscopic studies argued in favor of single coenzyme Q and cytochrome *c* pools (Blaza et al., 2014; Trouillard et al., 2011), and a definitive demonstration that quinone and quinol diffuse freely in and out of SCs has recently come from studies that incorporated an alternative quinol oxidase into mammalian heart mitochondrial membranes and showed to establish a competing pathway for quinol oxidation (Fedor and Hirst, 2018). Therefore, the catalytic relevance of the SCs remains questioned (Lobo-Jarne and Ugalde, 2018; Milenkovic et al., 2017). In addition, the $I+III_2+IV_n$ respirasomes have been proposed to stabilize CI (Moreno-Lastres et al., 2012; Scha¨ gger et al., 2004) and to prevent the production of CI-derived reactive oxygen species (ROS) (Maranzana et al., 2013). The recently defined high-resolution cryoelectron microscopy (cryo-EM) reconstructions of the mammalian respirasome (Gu et al., 2016; Letts et al., 2016; Sousa et al., 2016; Wu et al., 2016) are expected to be instrumental to unveil the potential functional properties of the SCs. Structural studies of the SC $I+III_2+IV_1$ from bovine, ovine, and porcine heart mitochondria showed that CIV is positioned at the distal end of the membrane arm of CI and adjacent to $CIII_2$. In addition, structural analyses in HEK293 cells showed the first architecture of the human respirasome, as well as the arrangement of the MRC complexes in a novel circular structure termed the megacomplex $I_2+III_2+IV_2$ (Guo et al., 2017), where $CIII_2$ forms a central core surrounded by two copies each of CI and CIV. The availability of these structures has only reinforced the intrigue about the biogenetic mechanisms and players that trigger the formation of the SCs. Besides the presence of the phospholipid cardiolipin (Mileykovskaya and Dowhan, 2014), SCs formation requires the action of specific assembly factors both in yeast (Chen et al., 2012; Singhal et al., 2017; Strogolova et al., 2012; Vukotic et al., 2012) and mammals (Chen et al., 2012; Davoudi et al., 2016; Ikeda et al., 2013; Lapuente-Brun et al., 2013; Mourier et al., 2014; Pérez-Pérez et al., 2016), although their specific functions remain under debate.

A controversial case involves the role of the protein COX7A2- like (COX7A2L, SCAFI, or COX7RP), highly homologous to the CIV subunit COX7A. COX7A2L was initially proposed to be central for the inclusion of CIV in SCs III_2+IV and $I+III_2+IV_{1–4}$ (Lapuente-Brun et al., 2013). Two COX7A2L variants were detected in commonly used laboratory mouse strains: a full-length 113-amino acids (long) protein present in CD1 mice, and a 111-amino acids (short) protein present in the C57BL/6 and BALB/c strains that missed two conserved residues (V72-P73) important for its stability and function in SCs formation (Lapuente-Brun et al., 2013). However, several groups reported the presence of respirasomes in C57BL/6 mice (Barrientos and Ugalde, 2013; Ikeda et al., 2013; Lapuente-Brun et al., 2013; Mourier et al., 2014; Williams et al., 2016), and cultured human cells silenced for *COX7A2L* expression also showed a specific requirement of COX7A2L for SC III_2+IV

assembly but not for respirasomes accumulation (Pérez-Pérez et al., 2016). These studies highlighted the preferential interaction of COX7A2L with $CIII_2$ and to a minor extent with monomeric CIV (Pérez-Pérez et al., 2016), which suggested an additional CIII-related mechanism of action for COX7A2L. There is currently a consensus that the full-length COX7A2L is required to promote SC III_2+IV formation and that it does so by binding independently to both $CIII_2$ and CIV (Cogliati et al., 2016; Pérez-Pérez et al., 2016; Zhang et al., 2016). It is also agreed that COX7A2L depletion does not affect the accumulation of the respirasomes I+III_2+$IV_{1–4}$ in some mouse tissues such as heart, as well as in *COX7A2L*-silenced human cells (Mourier et al., 2014; Pérez-Pérez et al., 2016; Williams et al., 2016). Interestingly, the short COX7A2L iso- form in C57BL/6 mice induced tissue-specific differences in the levels of the larger respirasomes I+III_2+$IV_{2–4}$, which were less abundant in liver than in heart mitochondria (Williams et al., 2016). Even the respirasome I+III_2+IV_1 was shown to be unstable in some tissues according to some reports (Cogliati et al., 2016), but not to others (Davoudi et al., 2016; Mourier et al., 2014; Sun et al., 2016; Williams et al., 2016). Based on proteomics analyses of the SCs subunit composition, it was hypothesized that the expression of tissue-specific isoforms of CIV subunits (e.g heart-muscle/liver COX7A1/COX7A2) could substitute COX7A2L in the respirasomes, inducing slight structural alterations in the CIV holocomplex that would differentially affect the assembly of the SCs in the presence of a specific COX7A variant (Cogliati et al., 2016), a possibility that remains to be experimentally demonstrated.

To unambiguously determine the function of COX7A2L in the organization of the human respiratory chain, we have used transcription activator-like effector nucleases (TALENs) technology to generate stable human *COX7A2L*-knockout (*COX7A2L*-KO) lines in HEK293T and in glioblastoma U87 cells, which were complemented either with the wild-type (WT) human COX7A2L, or with a mutant variant carrying an in-frame 6-bp deletion similar to that previously identified in the C57BL/6 mouse strain. Our results confirm that WT (long) COX7A2L is specifically required for the assembly of SC III_2+IV and the accumulation of megacomplexes, but dispensable for respirasome (or SCs I+III_2+IV_1) biogenesis, and reconcile an array of previous observations. *De novo* assembly studies show that COX7A2L regulates the assembly kinetics of the respirasomes probably through the modulation of $CIII_2$ levels. Biochemical data also demonstrate that the mutant COX7A2L variant does not support SC III_2+IV assembly because, despite being able to bind to both $CIII_2$ and SC I+III_2, it cannot interact with CIV or CIV-containing SCs. Functional substrate competition assays showed no differences in mitochondrial respiration between control and *COX7A2L*-KO cells, even under conditions of nutritional, environmental, or oxidative cellular stress. We conclude that by preventing the formation of SC III_2+IV, COX7A2L establishes a checkpoint for the regulation of $CIII_2$ levels and its incorporation into specific SCs. Most importantly, COX7A2L promotes MRC remodeling without affecting mitochondrial bioenergetics.

RESULTS

TALEN-Mediated Generation of *COX7A2L*-KO Cell Lines

To determine the requirement of human COX7A2L for mitochondrial SCs formation, and specifically for the assembly of the respirasomes, we used the TALEN gene-editing approach (Christian et al., 2010; Li et al., 2011) to create stable human *COX7A2L*-KO lines in HEK293T (human embryonic kidney) cells. A TALEN pair was designed to target a region within the first exon of the *COX7A2L* gene immediately downstream the start codon (Figure 1A). We co-transfected HEK293T cells with the TALEN pair, and subsequently, single clones were isolated by size cell sorting and analyzed for mutations leading to COX7A2L protein loss. More than 100 clones were screened by immunoblotting from cell extracts using a specific anti- COX7A2L antibody. We selected five promising candidates that completely lack the COX7A2L protein (Figure 1B). The *COX7A2L* gene was sequenced in two of these clones and found to carry KO mutations. Clone KO1 (C2E11) is homozygous and clone KO2 (C1C3) is compound heterozygous, both carrying *COX7A2L* alleles with short deletions involving the start codon and leading to the complete absence of COX7A2L (Figure 1C).

COX7A2L-KO Cells Display Absence of SC III_2+IV with Normal Respirasome Levels and Increased $CIII_2$ Levels and Activity

To analyze the pattern of supramolecular assemblies of MRC complexes resulting from the total absence of COX7A2L in human cells, we performed a first exploration in digitonin-solubilized cell extracts from WT and *COX7A2L*-KO cells by blue native (BN)-PAGE followed by CI-in gel activity (IGA) and immunoblotting. Our results unambiguously show that human COX7A2L is essential for the formation of SC III_2+IV, but its loss does not affect the basic respirasome (or SCs I+III_2+IV_1) that accumulates equally in WT and KO cells (Figure 1D). Similar results were obtained when using mitochondria-enriched fractions from WT HEK293T, KO1, and KO2 clones (Figure 2A). However, some scarce SCs larger than the basic respirasome I+III_2+IV_1, occasionally appeared to be at lower levels in some experiments with HEK293T cells. These SCs could contain multiple CIV units (I +III_2+$IV_{2–4}$) but are also compatible with the recently described respiratory megacomplex I_2+III_2+IV_2 (Guo et al., 2017). For simplification, in the figures we have labeled them as MegaC (megacomplexes). The loss of these larger SCs was clearly re-produced in a different model of human *COX7A2L*-KO in U87 glioblastoma cells (see below), suggesting that these MRC structures fail to assemble in the absence of functional COX7A2L, but might also be more labile than in WT mitochondria.

To assess whether the stability of the respirasomes depends on COX7A2L, we exposed mitochondria-enriched fractions from WT and *COX7A2L*-KO cells to varying concentrations of digitonin and analyzed the extracts by BN-PAGE followed by CI- and CIV-IGAs or immunoblotting (Figure S1). Stringent SCs extraction conditions using increasing (4–40 mg/mg) digitonin-to-protein ratios (Figure S1A) led to a parallel disintegration of the respirasomes (SCs I+III_2+IV_n) and consequent accumulation of SC I +III_2 and free CI in both cell types. Only when we used an extremely harsh 40 mg/mg digitonin:protein ratio were the respirasomes slightly more unstable in *COX7A2L*-KO than

in WT cells. Milder SCs extraction conditions using decreasing (4–1 mg/mg) digitonin-to-protein ratios, revealed no differences in the levels of SC I+III_2+IV_1 between *COX7A2L*-KO and WT cells (Figure S1B), but a clear decrease in the abundance of larger SCs (indicated with an asterisk) in *COX7A2L*-KO cells (Figures 2A and 2B), further suggesting that COX7A2L may be required for the normal assembly or stability of these megastructures. On the contrary, the abundance and stability of monomeric and dimeric CIV were not affected by the absence of COX7A2L (Figures 2A and 2B).

We next used a two-dimensional (2D)-BN/SDS-PAGE system to analyze in detail the pattern of SCs in *COX7A2L*-KO cells and the co-localization of COX7A2L with all MRC structures in WT cells. Although we had previously reported that COX7A2L associates with pre-$CIII_2$ before the incorporation of the RISP subunit(Pérez-Pérez et al., 2016), RISP assembly is not affected in *COX7A2L*-KO cells as it was detected in $CIII_2$, and in SCs I+III_2 and I +III_2+IV_{1-n} (Figure 2A). However, the accumulation of $CIII_2$ was significantly increased by ~2-fold in the absence of COX7A2L (Figures 1D, 2A–2D, S1A, and S1B). The increase in $CIII_2$ levels was not only a consequence of redistribution from the unassembled SC III_2+IV. A boost in $CIII_2$ levels was detected when using *COX7A2L*-KO mitochondrial extracts prepared not only in the presence of digitonin but also in the presence of lauryl maltoside (Figure 2D), which disrupts SC integrity, indicating that the total amount of assembled $CIII_2$ is increased. In agreement, spectrophotometric measurements of MRC enzyme activities showed that CIII activity was specifically enhanced by ~40% in the KOs (Figure 2E), consistent with the accumulation of $CIII_2$ in these cells.

All of the phenotypes described in *COX7A2L*-KO cells in this section, particularly the absence of SC III_2+IV and the accumulation of $CIII_2$, were specific since they were restored by the over- expression of recombinant COX7A2L-Myc-DDK in both KOs (Figures S2A–S2C), thus eliminating the possibility of off-target effects that could have arisen during the *COX7A2L* gene disruption. Tagged-COX7A2L incorporated into the same MRC structures as the endogenous COX7A2L (Figure S2B), and its mild overexpression (2- to 3-fold) did not induce any aberrant pheno- type (Figure S2).

COX7A2L-KO Cells Display a Boost in $CIII_2$ Biogenesis in Parallel with Slower Respirasome Assembly Kinetics

We next analyzed the assembly kinetics of MRC complexes and SCs by doxycycline-induced reversible inhibition of mitochondrial translation in WT and *COX7A2L*-KO cells. Doxycycline was removed from the cell culture media after 6 days of treatment, and samples were collected at different time points (0, 6, 15, 24, 48, 72, and 96 hr). To follow the reappearance of newly assembled $CIII_2$, CIV, CIV_2, and SCs, digitonin-solubilized mitochondria were separated by BN-PAGE and subsequently analyzed by either CI-IGA assays (Figures 3A and 3B) or immunoblot using antibodies that recognize CORE2 (CIII), COX1 (CIV; not shown), and COX5A (CIV) (Figures 3C and 3D). Following 6 days of doxycycline treatment (time 0 hr), only residual levels of CI, CIV, and $CIII_2$ (5%–10% of untreated cells) were detected in either control or KO cells (Figures 3A–3D). The treatment did not affect CII levels, as expected, since CII lacks mtDNA-encoded subunits. Once mitochondrial translation resumed (times 6–96 hr), the SC III_2+IV formed *de novo* only in

the WT cells (Figures 3C and 3D). The levels of CIV and CIV_2 increased at similar rates in WT and *COX7A2L*-KO cells (Figures 3C and 3D), ruling out a role for COX7A2L in the biogenesis of this complex. On the contrary, the rate of $CIII_2$ biogenesis, as shown for its steady-state levels in Figure 2, was markedly faster in the KOs than in the WT cells (Figures 3C and 3D). These data indicate a deregulation of $CIII_2$ levels in the absence of COX7A2L, suggesting that this protein establishes a regulatory checkpoint in $CIII_2$ biogenesis. Immunoblot analysis of CIII subunit levels during the recovery from the doxycycline treatment (Figure 3E) and in the steady state (Figure 3F) showed no significant differences in the steady-state levels of CIII subunits between WT and KOs, which indicate that a larger pool of unassembled sub- units may exist in the WT cells. Therefore, we propose that the $CIII_2$ increase in the KOs is a consequence of a more efficient $CIII_2$ assembly/stability rather than increased *de novo* synthesis of CIII subunits. Strikingly, the reappearance of the respirasomes $I+III_2+IV_n$ was clearly delayed in the *COX7A2L*-KO cells (Figures 3A–3D), but it reached levels comparable to the WT at later time points (78–96 hr; Figures 3A–3D) and in the steady state (Figure 2). These results suggest that, although the lack of COX7A2L does not prevent the formation of the respirasomes, it hampers their assembly efficiency perhaps by increasing the threshold of $CIII_2$ levels required to start the process (Moreno-Lastres et al., 2012).

To validate the hypotheses raised from the doxycycline experiments, we took into account the current model for $CIII_2$ assembly (Figure 3G), which includes the binding of COX7A2L to pre-$CIII_2$ prior to the incorporation of subunits UQCRFS1 and UQCR11 (Ferna´ ndez-Vizarra and Zeviani, 2015; Pérez-Pérez et al., 2016). The process of $CIII_2$ biogenesis, however, is not known in detail. For example, it remains unclear at which stage $CIII_2$ dimerization occurs. Here, we performed import/assembly assays in isolated WT and *COX7A2L*-KO mitochondria with specific ^{35}S-methionine-radiolabeled CIII precursors synthesized *in vitro*, in the presence and absence of mitochondrial membrane potential (Figure 3H). We chose to synthesize and import RISP (UQCRFS1; Figure 3I) and UQCR11 (Figure 3J), two late assembly proteins that are known to incorporate after the binding of COX7A2L to pre-$CIII_2$. In WT mitochondria, UQCRFS1 and UQCR11 incorporated into several subcomplexes up to the $CIII_2$ and followed by later incorporation into SCs ($I+III_2$ and $I+III_2+IV_n$). In *COX7A2L*-KO mitochondria, UQCRFS1 and UQCR11 incorporated more efficiently into the same intermediates as well as into $CIII_2$ than in WT mitochondria. On the contrary, the incorporation signals of these two radiolabeled proteins into SCs were less marked in the KO than in WT cells. Together, our import data show enhanced incorporation of newly imported proteins into $CIII_2$ assembly intermediates and attenuated formation of $CIII_2$-containing SCs in the *COX7A2L*-KO, suggesting that endogenous $CIII_2$ biogenesis is preferentially boosted and assembly intermediates are more abundant in *COX7A2L*-KO than in WT mitochondria.

Mitochondrial Bioenergetics in *COX7A2L*-KO Cells Is Indistinguishable from WT in Normal Physiological Conditions or under CI Deficiency

To ascertain the functional consequences of COX7A2L and SC III_2+IV depletion, we performed high-resolution endogenous oxygraphy to measure coupled cell respiration in intact cells, which is unaffected in the *COX7A2L*-KO clones (not shown).

Furthermore, substrate-driven competition was determined by treating digitonin-permeabilized cells supplemented with NADH- linked substrates (pyruvate, glutamate, malate) and $FADH_2$-linked substrates (succinate, glycerol-3-phosphate), with specific inhibitors of CI (piericidin A or rotenone) or CII (malonate). This experimental procedure allowed us to determine the respective contribution of CI and CII in feeding the respiratory chain (RC) with electrons during uncoupled respiration (Figures 4A–4D). In contrast with previous results in liver mitochondria from C57BL/6 mice (Lapuente-Brun et al., 2013) and in line with results obtained by some of us in liver and heart mitochondria from C57BL/6J and C57BL/6N mice (Mourier et al., 2014), substrate-driven competition was not affected in the *COX7A2L*-KO clones. Also, no effect on respiration resulted from COX7A2L overexpression (Figures 4A–4D). These results indicate that, in standard cell culture conditions, neither COX7A2L nor SC III_2+IV have a sub- stantial functional effect on electron flow through the MRC.

In human cells, more than 90% of CI is present in the respirasomes and the SC III_2+IV only constitutes ~5% of the total amount of MRC structures (Moreno-Lastres et al., 2012). Taking this MRC organization into account, we contemplated that, by limiting the enzymatic activity of CI, we could discern whether the absence of SC III_2+IV and the accumulation of $CIII_2$ in the *COX7A2L*-KO clones affect substrate competitive oxidation. To induce a partial inhibition of CI activity, we first treated the cells with 10 nM rotenone, 1.2 mM piericidin A, or the control vehicle (0.05% or 8.5 mM ethanol) for 24 hr (Figure 4E). CI inhibition did not significantly alter the distribution of MRC complexes and SCs in WT or KO cells (Figure 4F). Piericidin A treatment resulted in a comparable ~50% decrease in pyruvate-glutamate-malate + succinate-glycerol-3-phosphate (G3P) oxidation and similar substrate contribution in WT and KO digitonin-per-meabilized cells (Figure 4G).

Mitochondrial Bioenergetics in *COX7A2L*-KO Cells Is Indistinguishable from WT under Nutritional or Environmental Stress

The faster $CIII_2$ biogenesis and slower respirasome assembly rate observed in *COX7A2L*-KO cells would be consistent with a role for COX7A2L in accelerating SCs assembly to attend physiological needs or to recover from insults that could damage MRC complexes. In fact, it has been proposed that COX7A2L is induced, incorporated into CIV, and then enhances CIV activity under cellular stress conditions such as endoplasmic reticulum (ER) stress or ischemia (Zhang et al., 2016). Therefore, we assessed whether stressed HEK293T *COX7A2L*-KO cells could reveal a bioenergetics role for COX7A2L. Preliminary tests informed us that HEK293T cells do not exhibit a robust response to general stresses such as heat shock (Figure S3A), and although they respond to oxidative stress (Figures S3D and S3E), COX7A2L is not induced in the conditions tested (Figure S3B). Among the several cell lines examined, glioblastoma U-87 exhibited the most robust stress response (Figures S3A and S3B) and was used to generate a new *COX7A2L*-KO (U- KO). Two U-KO clones were obtained (Figures S4A and S4B). Since they exhibited a similar phenotype that was fully complemented by *COX7A2L* reconstitution (Figures 5B, S3C, and S3D), U-KO1 was used for subsequent experiments.

The pattern of MRC complexes and SCs was similar in HEK293T and U87 WT cells. However, SCs and MegaCs seemed more abundant in U87 (Figures 5A and 5B). The absence of *COX7A2L* in U87 cells prevented the assembly of SC III_2+IV and enhanced $CIII_2$ levels (Figures 5A and 5B) and delayed the assembly of the respirasomes (Figure S4C) as seen in HEK293T cells. It further limited the accumulation of SCs larger than the basic respirasome SC I+III_2+IV_1, although the detection of some traces of these SCs in U-KO cells could reflect their instability rather than failed assembly (Figures 5A, 5B, S4C).

In U87 WT cells, COX7A2L protein levels were enhanced up to ~4 fold following 48 hr under nutritional stress induced by carbon source switch from glucose to galactose (Figures 5C and 5D), a paradigm known to stimulate mitochondrial energy metabolism (Rossignol et al., 2004). The existing MRC complexes and SCs in WT and U-KO cells were equally induced after 48 hr in galactose and remained high at 72 hr (Figure 5E), when COX7A2L levels in WT cells had already attenuated (Figure 5D). As expected, coupled and uncoupled oxidation of pyruvate- glutamate-malate + succinate-G3P in permeabilized cells was stimulated in WT cells, but also in U-KO cells, and no differences were observed in substrate contribution (Figure 5F). Therefore, COX7A2L does not have any evident impact in glucose-togalactose nutritional-stress-induced MRC biogenesis and mitochondrial bioenergetics.

Environmental stresses in U87 cells such as acute heat shock (1 hr at 42°C; Figures S3A–S3C) or exogenous oxidative stress (1 hr in the presence of 100 mM H_2O_2; Figures S3D–S3F) also induced COX7A2L 2–4 hr after the insult. Yet, these stresses and subsequent recovery did not modify the MRC organization significantly (Figures S3C and S3F). The exposition to H_2O_2 promoted the equal accumulation of a CORE2-containing sub-SC in U87 WT and U-KO cells (Figure S3F), which could be a SC degradation product. As a minor difference, a proportion of U-KO cells higher than that of WT died during the acute oxidative stress, but no differences were detected in the endogenous respiration of the surviving cells (Figure S3G). We conclude that the MRC remodeling induced by COX7A2L does not influence mitochondrial bioenergetics during acute cellular stress.

A Mutant COX7A2L Variant Carrying a 6-bp Deletion Present in C57BL/6 Mice Retains the Ability to Bind $CIII_2$ but Does Not Rescue SC III_2+IV Assembly

In humans, only one COX7A2L protein of 114 amino acids has been reported (https://www.uniprot.org/uniprot/O14548) that is homolog to the long COX7A2L variant present in CD1 mice (Pérez-Pérez et al., 2016). To explore the functionality in human cells of the short COX7A2L isoform present in C57BL/6 and BALB/c mouse strains (Lapuente-Brun et al., 2013; Mourier et al., 2014), we generated cell lines constitutively expressing either FLAG-tagged COX7A2L (long) or a mutant version (short) carrying a deletion of amino acids V72 and P73 of human COX7A2L (Figure 6A). Both variants were stably expressed in WT HEK293T and *COX7A2L*-KO cells, which yielded no major differences in the steady-state levels of RC subunits (Figure 6A). MRC organization analysis by 2D-BN/SDS-PAGE revealed that the short COX7A2L variant was imported into mitochondria, where it colocalized with $CIII_2$ and SC I+III_2, but not with any CIV-containing structure (Figure 6B), as previously reported (Pérez-Pérez et al., 2016). Whereas expression of the long COX7A2L

variant in *COX7A2L*-KO cells restored normal levels of $CIII_2$ and SC III_2+IV, the short variant did not (Figures 6B–6D). Our analyses further disclosed that the expression of either the long or the short COX7A2L variants did not affect the steady-state levels of the respirasomes (Figures 6C and 6D). Similar observations were made in U87 and U-KO cells (Figure 5B). Together, these results support our view (Pérez-Pérez et al., 2016) that the 2-amino acid deletion present in the short COX7A2L isoform prevents its association with CIV but does not affect its binding to $CIII_2$, an interaction that is not sufficient to promote the formation of the SC III_2+IV.

Overexpression of CIV-Subunit Tissue-Specific Isoforms in *COX7A2L*-KO Cells Neither Rescues SC III_2+IV Assembly nor Enhances Respirasome Levels

Studies in mice suggested that COX7A2L could regulate the formation or stability of the CIV-containing SCs III_2+IV and I+III_2+IV_{2-n} in a tissue-specific manner (Williams et al., 2016). The relative levels of these SCs were lower in liver than in heart mitochondria from C57BL/6 mice, carrying the short COX7A2L variant, which could be explained by the occurrence of tissue- specific CIV subunit isoforms. Six isoforms have been so far described for the nucleus-encoded COX subunits in mammals: three liver/heart-type pairs of subunits (COX6A1/COX6A2, COX7A2/COX7A1, and COX8–1/COX8–2), the lung-specific isoform COX4–2, and two testes-specific isoforms, COX6B and COX8–3 (Pierron et al., 2012). While heart (or muscle) isoforms are expressed in tissues with high aerobic capacity and abundant mitochondria, liver (or non-muscle) isoforms are found in tissues like brain, liver, and kidney that generally contain fewer mitochondria (Pierron et al., 2012).

An attractive hypothesis suggests that COX7A2L could be replaced by the CIV subunit COX7A2 in the respirasomes, thereby supporting the co-existence of alternative SCs in different tissues (Cogliati et al., 2016; Letts et al., 2016; Letts and Sazanov, 2017). To demonstrate whether the expression of tissue-specific isoforms of CIV subunits differentially affects the assembly of the SCs in the absence of COX7A2L, we attempted to induce the formation of ‘‘tissue-specific’’ CIV in WT HEK293T and *COX7A2L*-KO cells, which constitutively express the CIV liver isoforms. To induce the formation of a ‘‘heart-type’’ CIV, we overexpressed either FLAG-tagged COX6A2 or COX7A1, and to induce a ‘‘lung-type’’ CIV, we overexpressed COX4i2 in both cell types (Figures S5A–S5C). We also analyzed the effect of COX7A2 overexpression in *COX7A2L*-KO cells (Figures S5A– S5C). None of the isoforms rescued the formation of SC III_2+IV or clearly altered the levels of the respirasomes (Figure S5D).

DISCUSSION

The biochemical and functional characterization of *COX7A2L*- KO human cell lines presented in this manuscript provide significant insights into the regulation of the MRC structural organization and respiratory metabolism by human COX7A2L. Our data help to clarify conflicting results on COX7A2L function that were primarily obtained in mouse models (Davoudi et al., 2016; Ikeda et al., 2013; Lapuente-Brun et al., 2013; Mourier et al., 2014; Pérez-Pérez et al., 2016; Williams et al., 2016). In this work, we demonstrate the role of COX7A2L in the coordinated regulation of $CIII_2$ and SCs biogenesis. We unambiguously

show that COX7A2L is essential to promote the assembly of SC III_2+IV in human cells, and also the accumulation of large SCs compatible with either respirasomes containing several copies of CIV ($I+III_2+IV_{2-n}$) or with the recently described MegaC ($I_2+III_2+IV_2$) (Guo et al., 2017). In contrast, COX7A2L is dispensable for the formation of the basic respirasomes (SCs $I+III_2$ and $I+III_2+IV_1$), although its absence hampers the assembly efficiency of these MRC structures, thus providing an explanation to the previous controversy. Importantly, COX7A2L establishes a regulatory checkpoint that specifically limits the accumulation of $CIII_2$. Physiologically, this adaptation of MRC organization and abundance promoted by COX7A2L is not essential to cope with nutritional, metabolic, or environmental cellular stresses and does not offer an obvious bioenergetics advantage, in contrast with a previous report (Lapuente-Brun et al., 2013). These concepts are depicted in a model presented in Figure 7 and are discussed below.

COX7A2L was originally presented as a SC assembly factor essential for the incorporation of CIV into SCs III_2+IV and $I+III_2+IV_{1-n}$ in mice (Lapuente-Brun et al., 2013). In C57BL/6 and BALB/c mouse strains, the lack of residues V72-P73 in a short COX7A2L variant was found to impact COX7A2L stability and its role in the assembly of CIV-containing SCs, including SC III_2+CIV and the respirasomes (Lapuente-Brun et al., 2013). In contrast, the results presented here show that, whereas the SC III_2+IV is not formed in human *COX7A2L*-KO cells, the respirasomes $I+III_2+IV_{1-n}$ accumulate to normal levels, consistent with previous data (Davoudi et al., 2016; Mourier et al., 2014; Pérez-Pérez et al., 2016; Williams et al., 2016), despite that they are assembled at a slower rate. However, SCs larger than $I+III_2+IV_1$ are unstable, particularly in U87 cells, in which MegaCs may fail to assemble. *In vivo*, the effect of COX7A2L in the SCs assembly rates may vary from tissue to tissue, which could be a contributing factor to explain why large respirasomes containing more than one CIV unit ($I+III_2+IV_{2-n}$) seem to be less abundant in liver than in heart from C57BL/6 mice (Williams et al., 2016).

Regarding the short COX7A2L variant, expression of a human version in *COX7A2L*-KO cells does not support SC III_2+IV assembly, as seen in C57BL/6 mice (Lapuente-Brun et al., 2013),and it does not affect the steady-state levels of SCs $I+III_2+IV_{1-n}$. Importantly, whereas the short variant retains the ability to bind both $CIII_2$ and SC $I+III_2$, it does not interact with CIV or CIV-containing respirasomes. In contrast, WT (long) COX7A2L preferentially co-segregates with monomeric CIV, with SCs III_2+IV and the respirasomes, and, to a minor extent, with $CIII_2$ in human HEK293T cells, as it occurs in mouse heart mitochondria and in human 143B osteosarcoma cells (Pérez-Pérez et al., 2016). These data are consistent with the views that COX7A2L associates with $CIII_2$ and CIV through independent domains to form the SC III_2+IV (Cogliati et al., 2016; Pérez-Pérez et al., 2016; Zhang et al., 2016), and that COX7A2L binding to CIV requires the correct orientation of a histidine residue at position 73 (Cogliati et al., 2016). Altogether, these results suggest that COX7A2L promotes specific interactions between $CIII_2$ and CIV that are essential for their association into SC III_2+IV, which are probably different to their interactions in the respirasomes, where CI is recruited into the macrostructure (Gu et al., 2016; Letts et al., 2016; Sousa et al., 2016; Wu et al., 2016). This supports the hypothesis that different pathways may operate to assemble the different SCs (Letts and Sazanov, 2017). SC III_2+IV and MegaCs could be assembled by the coming together of the individual complexes, which requires COX7A2L. In contrast, SC

$I+III_2+IV_1$ would be assembled in a COX7A2L-independent manner, compatible with the incorporation of newly synthesized sub- units/subassemblies from $CIII_2$ and CIV that accumulate once these fully assembled complexes have reached their steady- state levels, into larger structures containing CI intermediates, as we previously proposed (Moreno-Lastres et al., 2012).

In our model, the deregulation in the $CIII_2$ steady-state levels provoked by the absence of COX7A2L would delay the formation of the basic $I+III_2+IV_1$ respirasome, as well as the further incorporation of additional fully assembled CI or CIV units to generate larger respirasomes or MegaCs. The significant accumulation of $CIII_2$ levels was restored to normal by complementation with the long-COX7A2L variant, but not with the short variant, despite its retention of the ability to bind the complex. In this vein, we previously reported that, in cybrid cell lines lacking $CIII_2$, the stability of COX7A2L is largely compromised (Pérez-Pérez et al., 2016). Furthermore, *de novo* assembly studies in control 143B cells indicated that COX7A2L assembles into a pre-$CIII_2$ before the incorporation of the catalytic RISP subunit, whereas COX7A2L only binds CIV once this complex is fully assembled (Pérez-Pérez et al., 2016). These negative genetic interactions initially suggested an indirect regulatory role for COX7A2L in regulating $CIII_2$ assembly or stability, most probably through the biogenesis of SC III_2+IV. In this work, we have further demonstrated that the loss of COX7A2L enhances the *de novo* synthesis of $CIII_2$ in detriment of the respirasomes, and therefore COX7A2L establishes a threshold to the accumulation of $CIII_2$ in the steady state required to ignite respirasome assembly (Moreno-Lastres et al., 2012).

Finally, the impact of the MRC structural remodeling promoted by COX7A2L on mitochondrial physiology has also been a source of controversy. It was proposed that COX7A2L-dependent SC organization remodeling provides a mechanism for the physiological regulation of energy metabolism in mammals by providing alternate paths for electrons derived from the catabolism of specific substrates (Lapuente-Brun et al., 2013). In this model, electron flux from CI to $CIII_2$ (carried by NADH) would proceed essentially within the CI-containing SCs, whereas electron flow from CII (carried by FAD) would preferentially occur through free $CIII_2$ and SC III_2+IV (Lapuente-Brun et al., 2013). ATP production and respiration rates were found higher in mouse liver mitochondria and permeabilized fibroblasts with the unstable short-COX7A2L variant, both in the presence of pyruvate + malate (NADH-linked substrates) or succinate (FAD-linked substrate), whereas maximal respiration and ATP production in cells expressing long-COX7A2L required substrates for both electron transfer paths (Lapuente-Brun et al., 2013). However, other groups reported lower mitochondrial respiration and ATP synthesis in muscle (Ikeda et al., 2013) and liver (Shiba et al., 2017) from *COX7A2L*-KO mice or no effect of short-COX7A2L on mouse heart mitochondrial respiration (Mourier et al., 2014). Our human *COX7A2L*-KO cellular models displayed no differences with WT cells in coupled endogenous cell respiration, or in single and combined substrate (pyruvate- glutamate-malate or succinate-G3P) oxidation, indicating a minor functional role of COX7A2L in normal cultured cell physiological conditions. Similar results were obtained when the cultures were exposed to several nutritional, oxidative, and environmental cellular stresses, even though they actually induce COX7A2L protein by 4- to 10-fold. Altogether, our results contest the highly controversial role of COX7A2L in MRC SCs organization that has been

hypothesized to maximize mitochondrial bioenergetics efficiency (Bianchi et al., 2004; Lapuente-Brun et al., 2013).

A potential caveat of our studies is the use of cell culture models, which are maintained in conditions that could differ *in vivo*, particularly regarding tissue oxygen and nutrient availabilities. However, similar results were obtained in two different cell models and an array of culture conditions. Our data serve to clarify some of the current discrepancies regarding the impact of COX7A2L on the organization and function of the MRC complexes. We conclude that the role of COX7A2L in SC III_2+IV assembly, which is well established in the literature, and in the assembly/stability of higher SCs or MegaCs, has no impact in mitochondrial bioenergetics in any of the conditions tested. One could claim that the excess of free $CIII_2$ that accumulates when SC III_2+IV is absent could compensate for the instability of MegaCs and the slower SC assembly kinetics observed in *COX7A2L*-KO cells, but if this occurs, it is not via preferential substrate utilization, as also supported by other groups (Blaza et al., 2014; Fedor and Hirst, 2018; Trouillard et al., 2011). Alternatively, COX7A2L could be part of a response to accelerate CIII- containing SCs assembly when needed to preserve stability of individual complexes (Acı´n-Pérez et al., 2004) or to minimize ROS production (Maranzana et al., 2013), possibilities that warrant future research efforts.

STAR★METHODS

KEY RESOURCES TABLE

REAGENT or RESOURCE	SOURCE	IDENTIFIER
Antibodies		
ATP5A	Abcam	Cat# ab14748 RRID: AB_301447
β-ACTIN	Abcam	Cat# ab8227 RRID: AB_2305186
BCS1-L	Abcam	Cat# ab102808 RRID: AB_10859410
CORE1	Abcam	Cat# ab110252 RRID: AB_10863633
CORE2	Abcam	Cat# ab14745 RRID: AB_2213640
COX1	Abcam	Cat# ab14705 RRID: AB_2084810
COX2	Abcam	Cat# ab110258 RRID: AB_10887758
COX4I1	Abcam	Cat# ab14744 RRID: AB_301443
COX4I2	Abcam	Cat# ab70112 RRID: AB_2085283
COX5A	Sigma	Cat# HPA027525
COX5B	Santa Cruz	Cat# sc-374417 RRID: AB_10988066
COX6A1	Sigma	Cat# HPA062394 RRID: AB_2684749
COX6A2	Abcam	Cat# ab103139 RRID: AB_10710958
COX7A1	Abcam	Cat# ab134989
COX7A2L	ProteinTech	Cat#11416–1-AP RRID: AB_2245402
FLAG-tag	Sigma	Cat# F3165 RRID: AB_259529
HSP70 (HSPA6)	Origene	Cat# TA501950 RRID: AB_11124627
NDUFA9	Abcam	Cat# ab14713 RRID: AB_301431

REAGENT or RESOURCE	SOURCE	IDENTIFIER
NDUFS1	Abcam	Cat# ab52690 RRID: AB_2151096
RISP	Abcam	Cat# ab14746 RRID: AB_301445
SDHA	Abcam	Cat# ab14715 RRID: AB_301433
SOD2	Sigma	Cat# HPA001814 RRID: AB_1080134
TIM50	Abcam	Cat# ab109527 RRID: AB_10858241
TOM20	Santa Cruz	Cat# sc-11415 RRID: AB_2207533
b-TUBULIN	Sigma	Cat# C4585 RRID: AB_258868
UQCRB	Abcam	Cat# ab190360
VDAC1	Abcam	Cat# ab14734 RRID: AB_443084
2° Ab-mouse	Rockland Immunochemicals	Cat# 610–103-121 RRID: AB_218457
2° Ab-rabbit	Rockland Immunochemicals	Cat# 611–1302 RRID: AB_219720
Chemicals, Peptides, and Recombinant Proteins		
Dulbecco's Modified Eagle Medium (DMEM)	Invitrogen	Cat# 31966–047
Fetal bovine serum (FBS)	Sigma	Cat# 12303C
Lipofectamine 2000	Invitrogen	Cat# 1168019
Opti-MEM I Reduced Serum Medium	ThermoFisher #	Cat# 31985062
n-dodecyl-b-d-maltoside (DDM)	Sigma	Cat# 5172
Digitonin, High Purity	Calbiochem	Cat# 300410
Native PAGE 20X Running Buffer	Novex-Life Technologies	Cat# BN2001
Native PAGE 20X Cathode Buffer Additive	Novex-Life Technologies	Cat# BN2002
Critical Commercial Assays		
TNT T7 Quick Coupled Transcription/Translation System	Promega	Cat# L1170
SuperSignal West Femto Maximum Sensitivity Substrate	ThermoFisher	Cat# 34095
Experimental Models: Cell Lines		
HEK293T	ATCC	Cat# CRL-3216
Glioblastoma U87	ATCC	Cat# HTB-14
Oligonucleotides		
COX7A2L-short-Forward: GTTTTTCCAGAAAGCTGATGGT	Sigma	This paper
COX7A2L-short-Reverse: GCCTCGTTTCAGGTAGAC	Sigma	This paper
COX7A2L-KO-Forward: AAGTTAGGCGATCTTCGGGC	Sigma	This paper
COX7A2L-KO-Reverse: GCTCGGACATGAGAAGTGGC	Sigma	This paper
SAS1_Hs01:	Sigma	Cat# oligo 3019431149–000060
SAS1_Hs02:	Sigma	Cat# oligo 3019431149–000070
Recombinant DNA		
TAL Effector (F)- *COX7A2L:* TGGGCGTCATGTACTACAA	Invitrogen	N/A
TAL Effector (R)- *COX7A2L:* GCAGAAGTTGGCAGGAGCA	Invitrogen	N/A

REAGENT or RESOURCE	SOURCE	IDENTIFIER
UQCR11 in pReceiver-B31	GeneCopoeia	Cat# EX-I0287-B31
UQCRB in pReceiver-B31	GeneCopoeia	Cat# EX-F0223-B31
UQCRFS1 or RISP in pReceiver-B31	GeneCopoeia	Cat# EX-A3744-B31
COX7A2L- Myc-DDK in pCMV6-Entry	Origene	Cat# RC202697
COX7A1- Myc-DDK in pCMV6-Entry	Origene	Cat# RC201154
COX4I1- Myc-DDK in pCMV6-Entry	Origene	Cat# RC209374
COX4I2- Myc-DDK in pCMV6-Entry	Origene	Cat# RC209204
COX6A1- Myc-DDK in pCMV6-Entry	Origene	Cat# RC210485
COX6A2- Myc-DDK in pCMV6-Entry	Origene	Cat# RC206539
pCMV6-A-Entry-Hygro	Origene	Cat# PS100024
COX7A2L-Myc-DDK in pCMV6-A-Entry-Hygro	This paper	N/A
Software and Algorithms		
SPSS	IBM, v 21.0	N/A
ImageJ	NIH	https://imagej.nih.gov/ij/
GraphPad Prism	GraphPad Software v.5.0a	N/A
ImageLab	BioRad, v 6.0.1	N/A
Other		
Pre-cast NuPAGE 4%–12% Bis-Tris gels	Invitrogen	Cat# NP0321BOX
Pre-cast NativePAGE 3%–12% Bis-Tris gels	Invitrogen	Cat# BN2011BX10

CONTACT FOR REAGENT AND RESOURCE SHARING

Further information and requests for resources and reagents should be directed to and will be fulfilled by the Lead Contact, Dr. Antoni Barrientos, Ph.D. (abarrientos@med.miami.edu).

EXPERIMENTAL MODEL AND SUBJECT DETAILS

Human cell lines, transfection and cell culture—HEK293T (CRL-3216) and glioblastoma U-87 (HTB-14) cells were obtained from ATCC and cultured in high-glucose Dulbecco's modified Eagle's medium (DMEM, Life Technologies) supplemented with 10% fetal bovine serum (FBS), 2 mM L-glutamine, 1 mM sodium pyruvate, 50 mg/ml uridine and antibiotics at 37°C under 5% CO_2. Analysis for mycoplasma contamination was routinely performed.

Nutritional and environmental stress conditions—For some experiments cells were exposed to nutritional, OXPHOS bioenergetics an environmental stressors. Nutritional stress was induced by transferring cells from glucose-containing to galactose-containing media and samples were analyzed over increasing times (12 to 48 hours). OXPHOS bioenergetics stress was induced with MRC complex I inhibitors: cells were exposed to 10 nM rote- none, 1.2 mM piericidin A or the control vehicle (0,05% or 8,5 mM ethanol) for 24 hours. Heat stress was induced by exposing cultures to 42°C for 1 hour and oxidative stress by supplementing the media with 100 mM H_2O_2 for 1 hour. Following heat or oxidative stress, the media was

changed and the cultures incubated in non-stress conditions before samples were collected after increasing times of recovery (0 to 8 hours).

METHOD DETAILS

Key reagents—Tables presenting the list of antibodies, recombinant DNAs, oligonucleotides and siRNA oligoribonucleotides used in this study are included in the supplementary material.

Plasmid transfection—To create stable human *COX7A2L* knockout (KO) lines in HEK293T and U87 cells, we used a pair of TALEN constructs obtained from Thermo-Invitrogen. The left and right TALEN of the pair were designed to target the TGGGCGTCATGTACTACAA and the GCAGAAGTTGGCAGGAGCA DNA sequences, respectively, at the *COX7A2L* locus (see key reagents tables). HEK293T or U87 cells grown on a 6-well plate at 30% confluency were transfected with 4 mg of the right and left TALEN plasmids as a pair using 5 mL of Lipofectamine 2000 (Thermo Fisher) pre-incubated in 300 mL of Opti-MEM (ThermoFisher). After 4 hours of incubation, the media were changed to complete DMEM medium. After 3–6 times of repetitive transfections every three days, cells were collected, diluted in complete DMEM medium and seeded as single cells in multiple 96 well plates. In some repetitions, single cells were isolated using Fluorescence Activated Cell Sorting (FACS). The surviving colonies screened by immunoblotting against COX7A2L and by genotyping, as reported (Bourens et al., 2014). For genotyping, *COX7A2L* was sequenced using oligonucleotides *COX7A2L*-KO-Forward and *COX7A2L*-KO-Reverse (see Key resources table)

The *COX7A2L*-KO cell lines were reconstituted with Myc-DDK-tagged variants (long or short) of COX7A2L. *COX7A2L*-Myc-DDK was cloned under the control of a CMV promoter in the pCMV6-A-Entry-Hygro plasmid (Origene, PS100024) using *Sfa*AI and *Mss*I sites. The short version of mouse COX7A2L comprises an in-frame 6 base pair deletion that led to the absence of 2 amino acids (V72 and P73) (Lapuente-Brun et al., 2013). To generate the short variant of human COX7A2L, we used the Q5® Site-Directed Mutagenesis Kit from NEB. ~20 ng of template DNA extracted from HEK293T cells were used, along with the primers COX7A2L-short-F: 5^0-GTTTTTCCAGAAAGCTGATGGT-3^0 (forward) and COX7A2L-short-R: 5^0-GCCTCGTTTCAGGTAGAC-3^0 (reverse), designed to flank the region to be deleted. After exponential amplification and the treatment with kinase and ligase, 5 ml of the reaction were transformed NEB 5-alpha competent *E.coli* cells using the pCMV6-A-Entry-Hygro plasmid (Origene).

For transfection of COX7A2L-Myc-DDK-Hygro constructs, we used 10 mL of Lipofectamine™ (Thermo Fisher) mixed with 4 mg of vector DNA in OPTIMEM-I media (GIBCO) according to the manufacturer's instructions. Two days after transfection, the media was supplemented with 200 mg/ml of hygromycin and drug selection was maintained for at least 21 days.

Whole Cell extracts and Mitochondrial isolation—Whole cell extracts were obtained by solubilization in RIPA buffer (25 mM Tris-HCl pH 7.6; 150 mM NaCl; 1% NP-40; 1% sodium deoxycholate and 0.1% SDS) with 1 mM PMSF and 1x mammalian protease

inhibitor cocktail (Sigma). Extracts were cleared by 5 minutes centrifugation at 10,000 g at 4°C.

Mitochondria-enriched fractions were isolated from at least ten 80% confluent 175 cm^2 flasks as described previously (Bourens et al., 2014; Ferna´ ndez-Vizarra et al., 2010; Moreno-Lastres et al., 2012). To extract mitochondrial proteins in native conditions, mitochondria were pelleted and solubilized in 200 mL buffer containing 1.5 M aminocaproic acid and 50 mM Bis-Tris (pH 7.0). After optimizing solubilization conditions, we decided to use digitonin at a concentration of 4 g/g protein. In some experiments, lauryl maltoside (LM) was used at 1%. Solubilized samples were incubated on ice for 15 min and centrifuged for 30 min at 10,000 xg at 4°C, and the supernatant was combined with 20 mL of sample buffer (750 mM aminocaproic acid, 50 mM Bis-Tris, 0.5 mM EDTA, 5% Serva Blue G-250) prior to loading.

Blue Native Electrophoresis and In-Gel Activity Assays—Native PAGE Novex® 3%–12% Bis-Tris Protein Gels (Life Technologies) gels were loaded with 60–80 mg of mitochondrial protein or 400 mg of total cell extracts prepared in the presence of either lauryl maltoside (LM) or digitonin at the protein-detergent ratios indicated in the figure legends. After electrophoresis, proteins were transferred to PDVF or nitrocellulose membranes and used for immunoblotting. Duplicate gels were further used for *in-gel* activity (IGA) assays and for second-dimension (2D) 10% SDS-PAGE gels.

SDS-PAGE and immunoblotting—Protein concentration was measured with the BCA reagent (Thermo Scientific). 20–60 mg of mitochondrial protein extract was separated by SDS–PAGE in the Laemmli buffer system (Laemmli, 1970). Then, proteins were transferred to nitrocellulose membranes at 40 V overnight and probed with specific primary antibodies listed in the Key reagents Table. Peroxidase-conjugated anti-mouse and anti-rabbit IgGs were used as secondary antibodies (Molecular Probes). Immunoreactive bands were detected with an ECL prime Western Blotting Detection Reagent (Amersham) in a ChemiDoc MP Imager (Biorad) or by exposition to X-ray films. Optical densities of the immunoreactive bands were measured using the ImageLab (Biorad) software or the ImageJ software in digitalized images.

Characterization of the mitochondrial respiratory chain and oxidative phosphorylation system—Mitochondrial respiratory chain enzyme activities were performed according to established methods (Medja et al., 2009), and expressed relative to the citrate synthase activity.

Endogenous cell respiration was measured polarographically at 37°C using a Clark-type electrode from Hansatech Instruments (Norfolk, United Kingdom). Substrate-driven respiration was assayed in digitonin-permeabilized cultured cells as reported (Barrien-tos et al., 2009). Briefly, trypsinized cells were washed with permeabilized-cell respiration buffer (PRB) containing 0.3 M mannitol, 10 mM KCl, 5 mM $MgCl_2$, 0.5 mM EDTA, 0.5 mM EGTA, 1 mg/ml BSA and 10 mM KH_3PO_4 (pH 7.4). The cells were resuspended at ~4 3 10^6 cells/ml in 1.5 mL of the same buffer air-equilibrated at 37 °C supplemented 10 units of

hexokinase and 2 mM ADP. One ml of cell suspension was immediately placed into the polarographic chamber to measure endogenous respiration.

High-resolution oxygen consumption rate of digitonin-permeabilized cells was performed as described previously (Silva Ramos et al., 2016) at 37^{O}C, using 1 million cells diluted in 2 mL of respiratory buffer (120 mM sucrose, 50 mM KCl, 20 mM Tris-Base, 4 mM KH2PO4, 2 mM $MgCl_2$, 1 mM EDTA, pH 7.2) using an Oxygraph-2K (Oroboros). Briefly, cells were permeabilized with 0.02 mg/ml digitonin. The oxygen consumption rate under phosphorylating condition was assessed using either NADH-linked substrates (10 mM glutamate, 10 mM pyruvate and 5 mM malate), or FADH-linked substrates (10 mM succinate plus 5 mM glycerol-3-phosphate) in the presence of 2.5 mM ADP. The non-phosphorylating state was obtained after ATP synthesis inhibition using 0.75 mg/ml oligomycin. Mitochondrial respiration was uncoupled by successive addition of up to 0.4 mM CCCP to reach maximal oxygen consumption. To assess the contribution of NADH-linked and FADH-linked substrates to total oxygen consumption, respiration was assessed in the presence of both kinds of substrates. Subsequently, complex I and complex II activities were sequentially inhibited using respectively 1.2 mM piericidin A and 3 mM malonate. Afterward, 5mM of antimycin A was added to validate the mitochondrial origin of the oxygen consumption measured.

De novo mitochondrial respiratory chain complex and supercomplex assembly—To follow the assembly kinetics of MRC complexes and supercomplexes, we depleted cells of the structures containing mtDNA- encoded subunits by treating the cultures with doxycycline, a reversible inhibitor of mitochondrial translation as reported (Moreno-Lastres et al., 2012). We cultured WT (HEK293 or U87) control and *COX7A2L*-KO cells for 6 days in the presence of 15 mg/ml doxycycline. To follow the accumulation of newly synthesized MRC complexes and their further association into super complexes, samples were collected at different time points (0, 6, 15, 24, 48, 72, and 96 hours) after doxycycline removal. Digitonin- solubilized mitochondrial particles were separated by BN-PAGE and analyzed by immunoblotting.

Overexpression of Complex IV tissue-specific (liver and heart) subunit isoforms in COX7A2L-KO cells—Genes coding for selected liver and heart Complex IV subunit isoforms (*COX4I1. COX4I2, COX6A1, COX6A2, COX7A1* and *COX7A2*) were cloned in frame with a Myc-DDK-tag into pCMV6 plasmid carrying a hygromycin resistance cassette. Each construct was transfected into the *COX7A2L*-KO cell line, by using 10 mL of Lipofectamine™ (Thermo Fisher) mixed with 4 mg of vector DNA in OPTIMEM-I media (GIBCO), according to the manufacturer's instructions. Two days after transfection, the media was supplemented with 200 mg/ml hygromycin and drug selection was maintained for at least 21 days.

In organello import of radiolabelled recombinant proteins—Plasmids with CIII subunit ORFs for *in organello* import were obtained from GeneCopoeia™. pReceiver-B31 vectors have *UQCR11* (EX-I0287-B31) and *UQCRFS1 or RISP* (EX-A3744-B31) ORFs under the control of the T7 promoter. Radiolabeled UQCR11 and UQCRFS1 proteins were synthesized in the presence of [^{35}S]-methionine, using the TNT T7 Quick Coupled

Transcription/Translation System (Promega). Import experiments were performed by incubating radiolabeled precursor subunits with 200 mg of freshly isolated mitochondria prepared as reported (Ferna´ ndez-Vizarra et al., 2010) in presence 33 mL of import buffer (20 mM HEPES-KOH pH 7.4, 600mM mannitol, 16 mM $MgCl_2$, 5 mM ATP, 225 mM KCl, 0.1 mg/ml pyruvate kinase, 5 mM methionine and 3% (w/v) fatty acid-free bovine serum albumin) in a total volume of 200 ml in STE buffer (0.32 M sucrose, 1 mM EDTA, 10 mM Tris-HCl pH 7.4), at 37°C for increasing times (5 to 60 min). To assess import dependence of mitochondrial membrane potential, control samples were incubated with 10 mM of CCCP. For SDS-PAGE analysis, samples were split into two aliquots and treated with or without 100 mg/ml proteinase K (Sigma) for 20 min on ice, before stopping the reaction with 1 mM PMSF for 10 min. Mitochondria were pelleted at 8,000 xg for 8 min at 4°C and resuspended in 100 ml of STE buffer for their further analysis. For BN-PAGE analysis, mitochondria samples were subjected to protease treatment and pelleted before undergoing the analysis as described above.

QUANTIFICATION AND STATISTICAL ANALYSIS

Unless indicated, all experiments were performed at least in triplicate and results were presented as mean ± standard deviation (SD) of absolute values or percentages of control. Statistical *p* values were obtained by application of the Mann-Whitney *U* test using the SPSS v21.0 program. $p < 0.05$ was considered significant test (*$p < 0.05$; **$p < 0.01$; ***$p < 0.001$). Information on biological and technical replicates and statistical significance is included in the figure legends.

Supplementary Material

Refer to Web version on PubMed Central for supplementary material.

ACKNOWLEDGMENTS

We thank Carlos T. Moraes and Erika Fernandez-Vizarra for critical reading of the manuscript. This research was supported by NIH R01 Grants GM105781 (to A.B. and C.U.) and GM112179 (to A.B.), NIH R35 Grant GM118141 (to A.B.), MDA Grant MDA-381828 (to A.B.), AHA Development Grant 14SDG20040003 (to F.F.), and Instituto de Salud Carlos III-MINECO/European FEDER Funds Grants PI14–00209 and PI17–00048 (to C.U.). A.M. receives support from the AFM-Telethon (Trampoline Grant 19613) and ANR JCJC (ANR-16-CE14–0013).

REFERENCES

Acin-Perez R, and Enriquez JA (2014). The function of the respiratory super- complexes: the plasticity model. Biochim. Biophys. Acta 1837, 444–450. [PubMed: 24368156]

Acı´n-Pérez R, Bayona-Bafaluy MP, Ferna´ ndez-Silva P, Moreno-Loshuertos R, Pérez-Martos A, Bruno C, Moraes CT, and Enrı´quez JA (2004). Respiratory complex III is required to maintain complex I in mammalian mito-chondria. Mol. Cell 13, 805–815. [PubMed: 15053874]

Acı´n-Pérez R, Fernández-Silva P, Peleato ML, Pérez-Martos A, and Enriquez JA (2008). Respiratory active mitochondrial supercomplexes. Mol. Cell 32, 529–539. [PubMed: 19026783]

Barrientos A, and Ugalde C (2013). I function, therefore I am: overcoming skepticism about mitochondrial supercomplexes. Cell Metab 18, 147–149. [PubMed: 23931749]

Barrientos A, Fontanesi F, and Diaz F (2009). Evaluation of the mitochondrial respiratory chain and oxidative phosphorylation system using polarography and spectrophotometric enzyme assays. Curr. Protoc. Hum. Genet Chapter 19, Unit 19.13.

Bianchi C, Genova ML, Parenti Castelli G, and Lenaz G (2004). The mitochondrial respiratory chain is partially organized in a supercomplex assembly: kinetic evidence using flux control analysis. J. Biol. Chem 279, 36562–36569. [PubMed: 15205457]

Blaza JN, Serreli R, Jones AJ, Mohammed K, and Hirst J (2014). Kinetic evidence against partitioning of the ubiquinone pool and the catalytic relevance of respiratory-chain supercomplexes. Proc. Natl. Acad. Sci. USA 111, 15735–15740. [PubMed: 25331896]

Bourens M, Boulet A, Leary SC, and Barrientos A (2014). Human COX20 cooperates with SCO1 and SCO2 to mature COX2 and promote the assembly of cytochrome c oxidase. Hum. Mol. Genet 23, 2901–2913. [PubMed: 24403053]

Chen YC, Taylor EB, Dephoure N, Heo JM, Tonhato A, Papandreou I, Nath N, Denko NC, Gygi SP, and Rutter J (2012). Identification of a protein mediating respiratory supercomplex stability. Cell Metab 15, 348–360. [PubMed: 22405070]

Christian M, Cermak T, Doyle EL, Schmidt C, Zhang F, Hummel A, Bogdanove AJ, and Voytas DF (2010). Targeting DNA double-strand breaks with TAL effector nucleases. Genetics 186, 757–761. [PubMed: 20660643]

Cogliati S, Calvo E, Loureiro M, Guaras AM, Nieto-Arellano R, Garcia-Poyatos C, Ezkurdia I, Mercader N, Vázquez J, and Enriquez JA (2016). Mechanism of super-assembly of respiratory complexes III and IV. Nature 539, 579–582. [PubMed: 27775717]

Cruciat CM, Brunner S, Baumann F, Neupert W, and Stuart RA (2000). The cytochrome bc1 and cytochrome c oxidase complexes associate to form a single supracomplex in yeast mitochondria. J. Biol. Chem 275, 18093–18098. [PubMed: 10764779]

Davoudi M, Kotarsky H, Hansson E, Kallija¨ rvi J, and Fellman V (2016). COX7A2L/SCAFI and pre-Complex III modify respiratory chain supercomplex formation in different mouse strains with a Bcs1l mutation. PLoS One 11, e0168774. [PubMed: 27997587]

den Dunnen JT, and Antonarakis SE (2000). Mutation nomenclature extensions and suggestions to describe complex mutations: a discussion. Hum. Mutat 15, 7–12. [PubMed: 10612815]

Fedor JG, and Hirst J (2018). Mitochondrial Supercomplexes do not enhance catalysis by quinone channeling. Cell Metab 28, 525–531.e4. [PubMed: 29937372]

Fernández-Vizarra E, and Zeviani M (2015). Nuclear gene mutations as the cause of mitochondrial complex III deficiency. Front. Genet 6, 134. [PubMed: 25914718]

Fernández-Vizarra E, Ferrı´n G, Pérez-Martos A, Fernández-Silva P, Zeviani M, and Enrı´quez JA (2010). Isolation of mitochondria for biogenetical studies: an update. Mitochondrion 10, 253–262. [PubMed: 20034597]

Gu J, Wu M, Guo R, Yan K, Lei J, Gao N, and Yang M (2016). The architecture of the mammalian respirasome. Nature 537, 639–643. [PubMed: 27654917]

Guo R, Zong S, Wu M, Gu J, and Yang M (2017). Architecture of human mitochondrial respiratory megacomplex I2III2IV2. Cell 170, 1247–1257.e12. [PubMed: 28844695]

Ikeda K, Shiba S, Horie-Inoue K, Shimokata K, and Inoue S (2013). A stabilizing factor for mitochondrial respiratory supercomplex assembly regulates energy metabolism in muscle. Nat. Commun 4, 2147. [PubMed: 23857330]

Laemmli UK (1970). Cleavage of structural proteins during the assembly of the head of bacteriophage T4. Nature 227, 680–685. [PubMed: 5432063]

Lapuente-Brun E, Moreno-Loshuertos R, Acı´n-Pérez R, Latorre-Pellicer A, Colás C, Balsa E, Perales-Clemente E, Quirós PM, Calvo E, Rodr´ıguez-Hernández MA, et al. (2013). Supercomplex assembly determines electron flux in the mitochondrial electron transport chain. Science 340, 1567–1570. [PubMed: 23812712]

Letts JA, and Sazanov LA (2017). Clarifying the supercomplex: the higher-order organization of the mitochondrial electron transport chain. Nat. Struct. Mol. Biol 24, 800–808. [PubMed: 28981073]

Letts JA, Fiedorczuk K, and Sazanov LA (2016). The architecture of respiratory supercomplexes. Nature 537, 644–648. [PubMed: 27654913]

Li T, Huang S, Zhao X, Wright DA, Carpenter S, Spalding MH, Weeks DP, and Yang B (2011). Modularly assembled designer TAL effector nucleases for targeted gene knockout and gene replacement in eukaryotes. Nucleic Acids Res 39, 6315–6325. [PubMed: 21459844]

Lobo-Jarne T, and Ugalde C (2018). Respiratory chain supercomplexes: structures, function and biogenesis. Semin. Cell Dev. Biol 76, 179–190. [PubMed: 28743641]

Maranzana E, Barbero G, Falasca AI, Lenaz G, and Genova ML (2013). Mitochondrial respiratory supercomplex association limits produc tion of reactive oxygen species from complex I. Antioxid. Redox Signal 19, 1469–1480. [PubMed: 23581604]

Medja F, Allouche S, Frachon P, Jardel C, Malgat M, Mousson de Camaret B, Slama A, Lunardi J, Mazat JP, and Lombe` s A (2009). Development and implementation of standardized respiratory chain spectrophoto-metric assays for clinical diagnosis. Mitochondrion 9, 331–339. [PubMed: 19439198]

Milenkovic D, Blaza JN, Larsson NG, and Hirst J (2017). The enigma of the respiratory chain supercomplex. Cell Metab 25, 765–776. [PubMed: 28380371]

Mileykovskaya E, and Dowhan W (2014). Cardiolipin-dependent formation of mitochondrial respiratory supercomplexes. Chem. Phys. Lipids 179, 42–48. [PubMed: 24220496]

Moreno-Lastres D, Fontanesi F, Garcı´a-Consuegra I, Martı´n MA, Arenas J, Barrientos A, and Ugalde C (2012). Mitochondrial complex I plays an essential role in human respirasome assembly. Cell Metab 15, 324–335. [PubMed: 22342700]

Mourier A, Matic S, Ruzzenente B, Larsson NG, and Milenkovic D (2014). The respiratory chain supercomplex organization is independent of COX7a2l isoforms. Cell Metab 20, 1069–1075. [PubMed: 25470551]

Pérez-Pérez R, Lobo-Jarne T, Milenkovic D, Mourier A, Bratic A, Garcı´a-Bartolomé A, Fernández-Vizarra E, Cadenas S, Delmiro A, Garcı´a-Consuegra I, et al. (2016). COX7A2L Is a mitochondrial complex III binding protein that stabilizes the III2+IV supercomplex without affecting respirasome formation. Cell Rep 16, 2387–2398. [PubMed: 27545886]

Pierron D, Wildman DE, Hu€ttemann M, Markondapatnaikuni GC, Aras S, and Grossman LI (2012). Cytochrome c oxidase: evolution of control via nuclear subunit addition. Biochim. Biophys. Acta 1817, 590–597. [PubMed: 21802404]

Rossignol R, Gilkerson R, Aggeler R, Yamagata K, Remington SJ, and Capaldi RA (2004). Energy substrate modulates mitochondrial structure and oxidative capacity in cancer cells. Cancer Res 64, 985–993. [PubMed: 14871829]

Schägger H, and Pfeiffer K (2000). Supercomplexes in the respiratory chains of yeast and mammalian mitochondria. EMBO J 19, 1777–1783. [PubMed: 10775262]

Schägger H, de Coo R, Bauer MF, Hofmann S, Godinot C, and Brandt U (2004). Significance of respirasomes for the assembly/stability of human respiratory chain complex I. J. Biol. Chem 279, 36349–36353. [PubMed: 15208329]

Shiba S, Ikeda K, Horie-Inoue K, Nakayama A, Tanaka T, and Inoue S (2017). Deficiency of COX7RP, a mitochondrial supercomplex assembly promoting factor, lowers blood glucose level in mice. Sci. Rep 7, 7606. [PubMed: 28790391]

Silva Ramos E, Larsson NG, and Mourier A (2016). Bioenergetic roles of mitochondrial fusion. Biochim. Biophys. Acta 1857, 1277–1283. [PubMed: 27060252]

Singhal RK, Kruse C, Heidler J, Strecker V, Zwicker K, Dusterwald L, Westermann B, Herrmann JM, Wittig I, and Rapaport D (2017). Coi1 is a novel assembly factor of the yeast complex III-complex IV supercomplex. Mol. Biol. Cell 9, Published online August 9, 2018. https://doi.org/10.1091/mbc.E17-02-0093.

Sousa JS, Mills DJ, Vonck J, and Ku€hlbrandt W (2016). Functional asymmetry and electron flow in the bovine respirasome. eLife 5, e21290. [PubMed: 27830641]

Strogolova V, Furness A, Robb-McGrath M, Garlich J, and Stuart RA (2012). Rcf1 and Rcf2, members of the hypoxia-induced gene 1 protein family, are critical components of the mitochondrial cytochrome bc1-cyto-chrome c oxidase supercomplex. Mol. Cell. Biol 32, 1363–1373. [PubMed: 22310663]

Sun D, Li B, Qiu R, Fang H, and Lyu J (2016). Cell type-specific modulation of respiratory chain supercomplex organization. Int. J. Mol. Sci 17, E926. [PubMed: 27338358]

Trouillard M, Meunier B, and Rappaport F (2011). Questioning the functional relevance of mitochondrial supercomplexes by time-resolved analysis of the respiratory chain. Proc. Natl. Acad. Sci. USA 108, E1027–E1034. [PubMed: 22011573]

Vukotic M, Oeljeklaus S, Wiese S, Vögtle FN, Meisinger C, Meyer HE, Zieseniss A, Katschinski DM, Jans DC, Jakobs S, et al. (2012). Rcf1 mediates cytochrome oxidase assembly and respirasome formation, revealing heterogeneity of the enzyme complex. Cell Metab 15, 336–347. [PubMed: 22342701]

Williams EG, Wu Y, Jha P, Dubuis S, Blattmann P, Argmann CA, Houten SM, Amariuta T, Wolski W, Zamboni N, et al. (2016). Systems proteomics of liver mitochondria function. Science 352, aad0189. [PubMed: 27284200]

Wu M, Gu J, Guo R, Huang Y, and Yang M (2016). Structure of mammalian respiratory supercomplex I1III2IV1. Cell 167, 1598–1609.e10. [PubMed: 27912063]

Zhang K, Wang G, Zhang X, Hu€ttemann PP, Qiu Y, Liu J, Mitchell A, Lee I, Zhang C, Lee JS, et al. (2016). COX7AR is a stress-inducible mitochondrial cox subunit that promotes breast cancer malignancy. Sci. Rep 6, 31742. [PubMed: 27550821]

Highlights

- *COX7A2L*-knockout human cells lack SC III_2+IV and some megacomplexes
- *COX7A2L*-KO cells have enhanced $CIII_2$ steady-state levels and assembly rate
- *COX7A2L*-KO cells have slower respirasome assembly but normal steady-state levels
- COX7A2L-dependent MRC remodeling does not affect mitochondrial bioenergetics

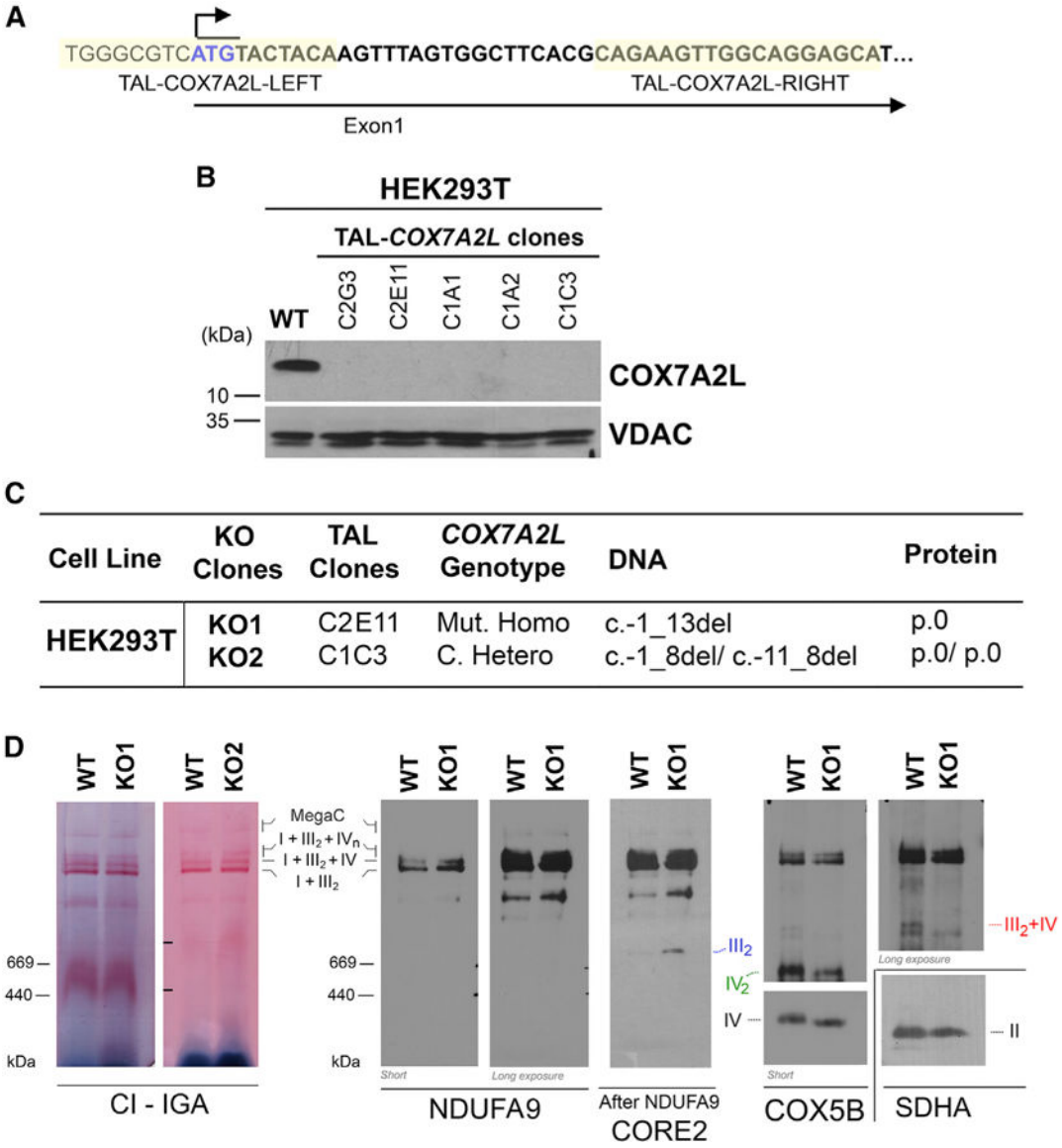

Figure 1. TALEN-Mediated Generation of COX7A2L-KO Clones in HEK293T Cells

(A) Schematic representation of the first exon of the *COX7A2L* locus and the sequences of recognition sites of the two TALEN pairs.

(B) Immunoblot analysis of the steady-state levels of COX7A2L in HEK293T (WT) and TALEN-transfected HEK293T cell lines. VDAC was used as a loading control.

(C) *COX7A2L* alleles in TAL-*COX7A2L* clones. The DNA numbering refers to the coding sequence (c.) and the protein (p.) number to the predicted full polypeptide (den Dunnen and Antonarakis, 2000). C, compound; Mut, mutant; Hetero, heterozygous; Homo, homozygous; del, deletion; -, position before starting ATG.

(D) BN-PAGE analysis of whole cells extracted with digitonin (detergent/protein ratio, 4:1) separated in a 4%–8% linear gradient polyacrylamide gel, followed by CI in-gel activity (IGA) or immunoblotting with the indicated antibodies. The identity of MRC complexes and

SCs is indicated in the margins. MegaC, megacomplexes probably containing more than one copy of CI, $CIII_2$, and CIV. See also Figure S1.

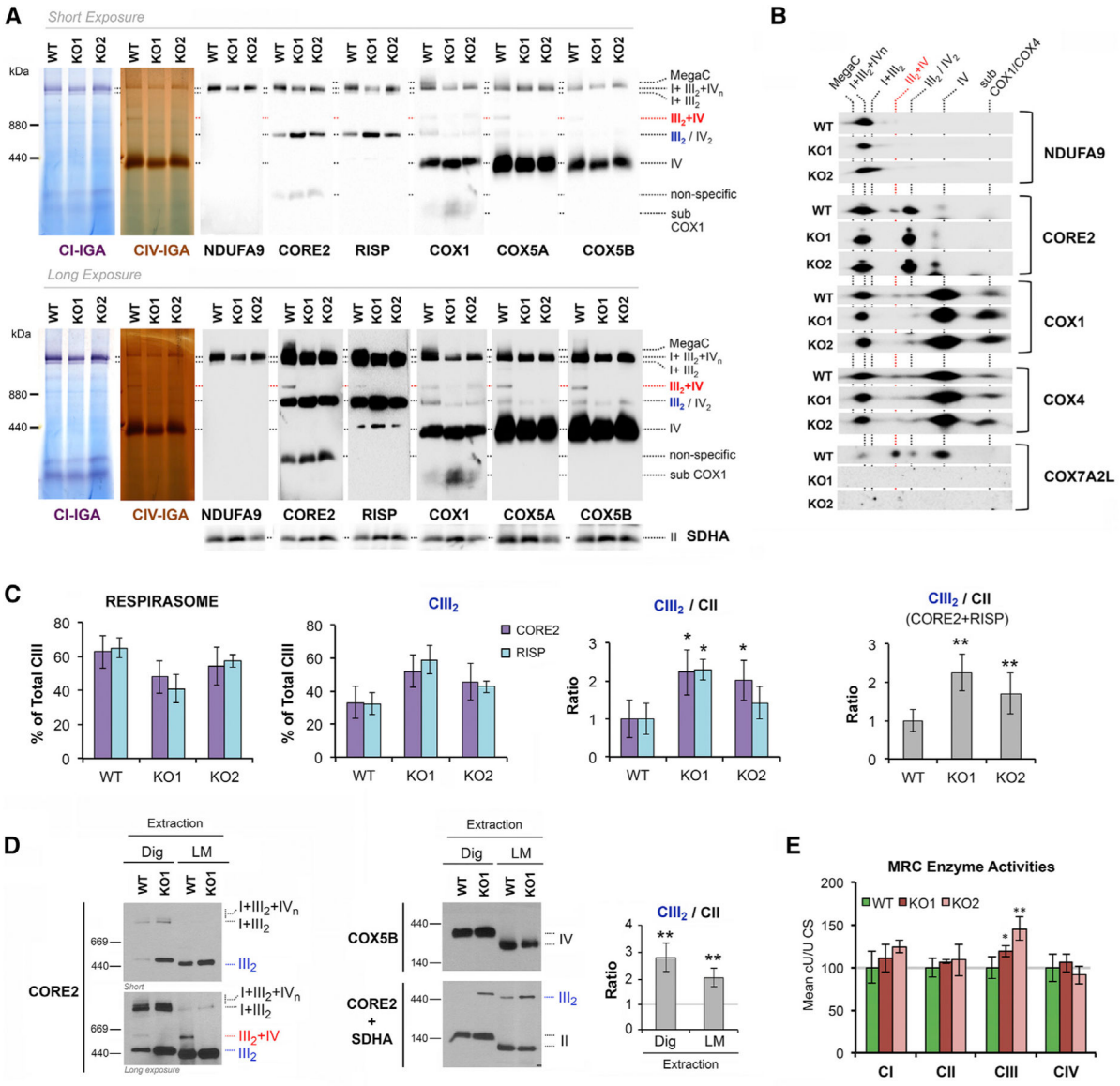

Figure 2. COX7A2L-KO Cells Display Absence of SC III2+IV with Normal Respirasome Levels and Altered Accumulation of CIII2

The effect of COX7A2L absence on MRC complex assembly was investigated in two *COX7A2L*-KO clones, clone 1 (KO1) and clone 2 (KO2), compared with the control HEK293T cells (WT).

(A) Mitochondria extracted with a digitonin/protein ratio of 4:1 (g/g) and analyzed by BN-PAGE, followed by CI- and CIV-IGA assays, or alternatively, by immunoblotting using the indicated antibodies.

(B) Subsequent 2D-BN/SDS-PAGE and immunoblot analyses were performed with antibodies against COX7A2L and the indicated OXPHOS subunits.

(C) To address the relative amount of $CIII_2$ in *COX7A2L*-KO cells, the signals from the CORE2 antibody from four BN-PAGE experiments were quantified by densitometry, normalized by CII, and indicated as mean ± SD.

(D) BN-PAGE analyses in whole-cell extracts prepared in the presence of digitonin (detergent/protein ratio, 4:1) or 1% lauryl maltoside (LM). The $CIII_2$ signals were quantified and normalized by CII using the histogram function of the Adobe Photoshop program on digitalized images, and the values were expressed relative to the control. Error bars represent the mean ± SD of four independent experiments.

(E) Spectrophotometric measurements of the individual activities of MRC complexes I to IV (CI–CIV) in WT and *COX7A2L*-KO cells. Enzyme activities are expressed as cU/U citrate synthase (CS). Error bars represent the mean ± SD of four repetitions. *$p < 0.05$; **$p < 0.01$. MegaC, megacomplexes probably containing more than one copy of CI, $CIII_2$, and CIV. $I+III_2+IV_n$, SCs containing CI, $CIII_2$, and CIV. $I+III_2$, SC containing CI and $CIII_2$. III_2+IV, SC containing $CIII_2$ and CIV. III_2, complex III dimer ($CIII_2$). IV, complex IV; IV_2, complex IV dimer (CIV_2). II, complex II. Subcomplexes that contain COX1 and COX4 are indicated. Apparent subcomplexes that contain CORE2 are antibody artifacts that disappear in 2D-BN/SDS-PAGE gels. See also Figure S2.

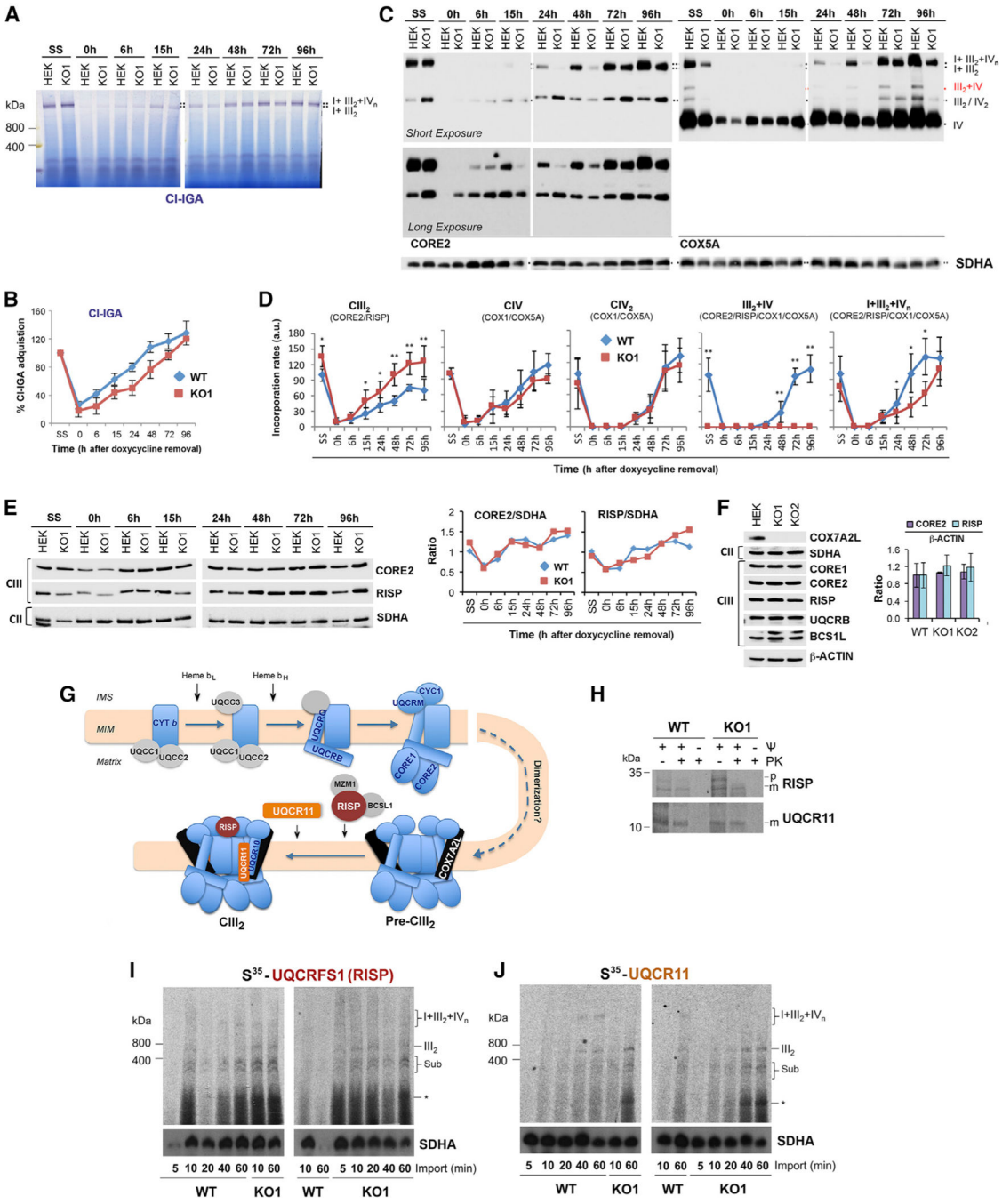

Figure 3. COX7A2L-KO Cells Have Enhanced Rate of De Novo CIII2 Biogenesis and Delayed Respirasomes Formation

(A–E) HEK293T (WT) and *COX7A2L*-KO clone 1 (KO1) cells were cultured for 8 days in the presence of 15 mg/mL doxycycline and collected at different time points (0, 6, 15, 24, 48, 72, and 96 hr) after doxycycline removal. Mitochondria prepared from these samples were extracted with a digitonin/protein ratio of 4 g/g and analyzed by BN-PAGE in combination with (A) CI-IGA assays or (C) immunoblotting with the indicated antibodies. (B) Mean CI activity recovery after doxycycline removal quantified from (A).

(C) Mean incorporation rates of CORE2 subunit in $CIII_2$, and of COX1 (not shown) and COX5A subunits in CIV and CIV_2, or their assembly kinetics in the $I+III_2+IV_{1-n}$ respirasomes.

(D) The signals from three independent experiments (as in C) for WT and KO cells were quantified and normalized by CII. Time point values are expressed as percentages of the untreated cells (SS) and indicated as means ± SD. *$p < 0.05$, **$p < 0.01$. $I+III_2+IV_n$, SCs containing CI, $CIII_2$, and CIV. III_2+IV, SC containing $CIII_2$ and CIV; III_2, complex III dimer ($CIII_2$); IV, complex IV; IV_2, complex IV dimer (CIV_2); II, complex II.

(E) For two doxycycline experiments, samples were analyzed by SDS-PAGE for the steady-state levels of CIII subunits CORE2 and RISP. On the right panel, the signals were quantified and plotted as ratio of SDHA. The values for the two independent experiments did not differ by more than 5%.

(F) Steady-state levels of the indicated CIII subunits in HEK293T WT, KO1, and KO2 cell lines. On the right panel, the signals of CORE2 and RISP were quantified and expressed as ratio of the signal of ACTIN, used as a loading control. Error bars represent the mean ± SD of three independent experiments.

(G) Simplified current model of CIII assembly depicting the order of subunit incorporation and time of dimerization, modified from Ferna´ ndez-Vizarra and Zeviani (2015).

(H) In organello import of the indicated recombinant proteins synthesized in a reticulocyte system in the presence of ^{35}S-methionine. The import assays were performed for 30 min in the absence or presence of the uncoupler CCCP to disrupt the mitochondrial membrane potential (J). Following import, an aliquot was treated with proteinase K to digest non-imported precursor proteins. M, mature; p, precursor.

(I and J) BN-PAGE analysis of the incorporation of the indicated radiolabeled recombinant proteins into CIII assembly intermediates, dimer, and SCs in HEK293T WT and KO1 cells during increasing times from 5 to 60 min. Import assays were performed in duplicates with similar results. Sub, subassemblies. The asterisk indicates small subassemblies that may correspond to the protein being imported bound to specific chaperones.

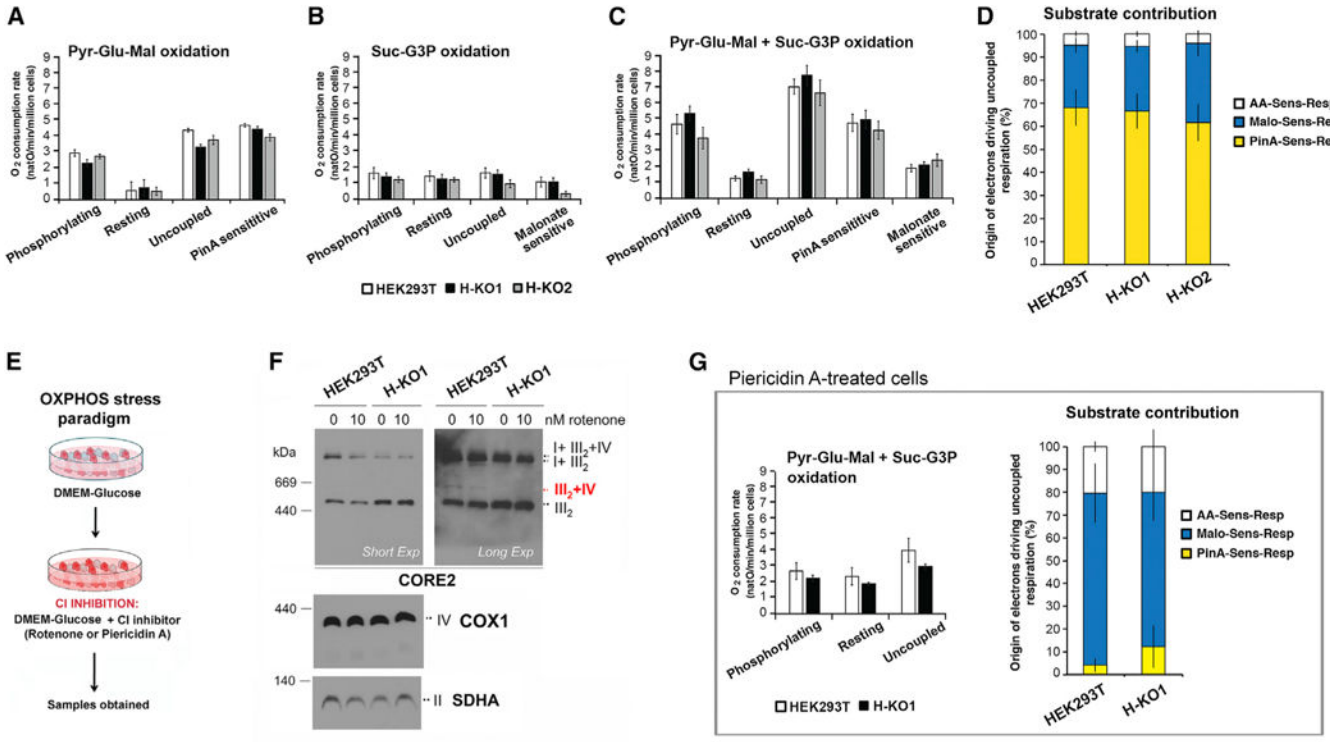

Figure 4. COX7A2L-KO Cells Are Capable of Normal OXPHOS Performance

Respiration of permeabilized *COX7A2L* KO and control HEK cells cultivated on DMEM high glucose (A–D) or DMEM high glucose supplemented with 1.2 mM piericidin A, a CI inhibitor (G).

(A) Respiration of digitonin-permeabilized HEK293T cells assessed in the presence of Pyr-Glu-Mal: pyruvate (10 mM), glutamate (10 mM), and malate (5 mM) under different respiratory states (phosphorylating, resting, and uncoupled) and piericidin A-sensitive respiration (PinA sens).

(B) Respiration of digitonin-permeabilized HEK293T cells assessed in the presence of Suc-G3P: succinate (10 mM) and glycerol-3-phosphate (5 mM) under different respiratory states (phosphorylating, resting, and uncoupled) and malonate-sensitive respiration (Malo sens).

(C) Respiration of digitonin-permeabilized HEK cells incubated with Pyr-Glu-Mal and Suc-G3P. The Piericidin A- (PinA sens) and Malonate-sensitive (Malo sens) respiration are determined under uncoupled conditions.

(D) Respective contribution of NADH and succinate dehydrogenases in providing electrons to sustain uncoupled respiration assessed with all substrates under uncoupled state.

(E) OXPHOS stress paradigm based on *in cello* CI inhibition with rotenone or piericidin A.

(F) Effect of 24-hr incubation in the presence of 50 nM rotenone in HEK293T WT and KO1 cells on SC stability, analyzed in digitonized cell extracts by BN-PAGE and immunoblotting with the indicated antibodies.

(G) Respiration analysis of HEK cells cultivated during 48 hr in presence of CI inhibitor (piericidin A). The respiration of digitonin-permeabilized cells incubated with Pyr-Glu-Mal and Suc-G3P assessed under different respiratory states (phosphorylating, resting, and uncoupled). The piericidin A (PinA sens)-, malonate (Malo sens)-, and remaining antimycin

A (AA)-sensitive respirations are determined under uncoupled conditions. The graph on the right side represents the respective contribution of CI and CII in providing electrons to sustain uncoupled respiration. In all the panels, error bars represent the mean ± SD of four biological repetitions. See also Figure S3.

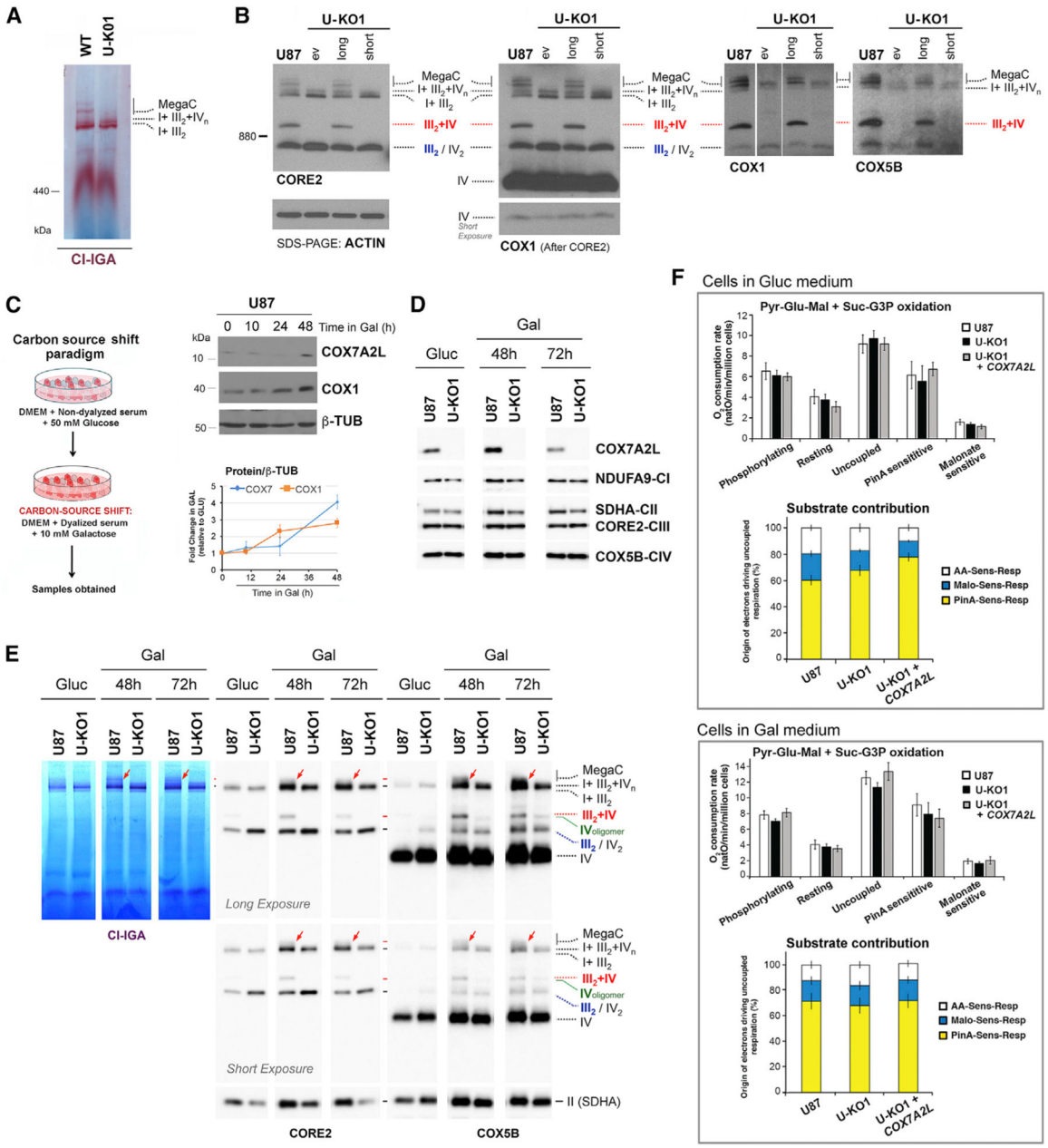

Figure 5. A Nutritional Challenge Induced by Switching the Carbon Source in the Media from Glucose to Galactose Does Equally Enhance Mitochondrial Bioenergetics Parameters in WT and COX7A2L-KO Cells

(A and B) Characterization of glioblastoma U87 WT and *COX7A2L*-KO (U-KO1) cells. The KO cells were stably transfected with an empty vector (ev) or constructs to express the long or short versions of COX7A2L. (A) and (B) show the BN-PAGE analysis of whole cells extracted with digitonin (detergent/protein ratio, 4:1) separated in a 4%–8% (A) or a 3%–12% (B) linear gradient polyacrylamide gel, followed by CI in-gel activity (IGA) (A) or immunoblotting with the indicated antibodies (B). The identity of MRC complexes and SCs is indicated in the margins. MegaC, megacomplexes probably containing more than one copy of CI, $CIII_2$, and CIV.

(C) Scheme depicting the carbon source switch paradigm used in this study.
(D) Time course quantification of COX7A2L induction by galactose in U87 WT cells. The graphs represent a quantification of the signals in three independent experiments, with error bars representing the mean ± SD.
(E) Mitochondria extracted with a digitonin/protein ratio of 4:1 (g/g) from cells grown in either glucose-containing (Gluc) or galactose-containing (Gal) medium and analyzed by BN-PAGE, followed by CI-IGA assays or, alternatively, by immunoblotting using the indicated antibodies. The red arrows indicate MegaCs exclusively detected in WT cells.
(F) Respiration of glioblastoma U87 cells assessed under different respiratory states (phosphorylating, resting, and uncoupled) and respective contribution of NADH and succinate dehydrogenases to the uncoupled respiration cultured in DMEM-glucose (upper panel), or DMEM-galactose (lower panel). Error bars represent the mean ± SD of four biological repetitions. See also Figure S4.

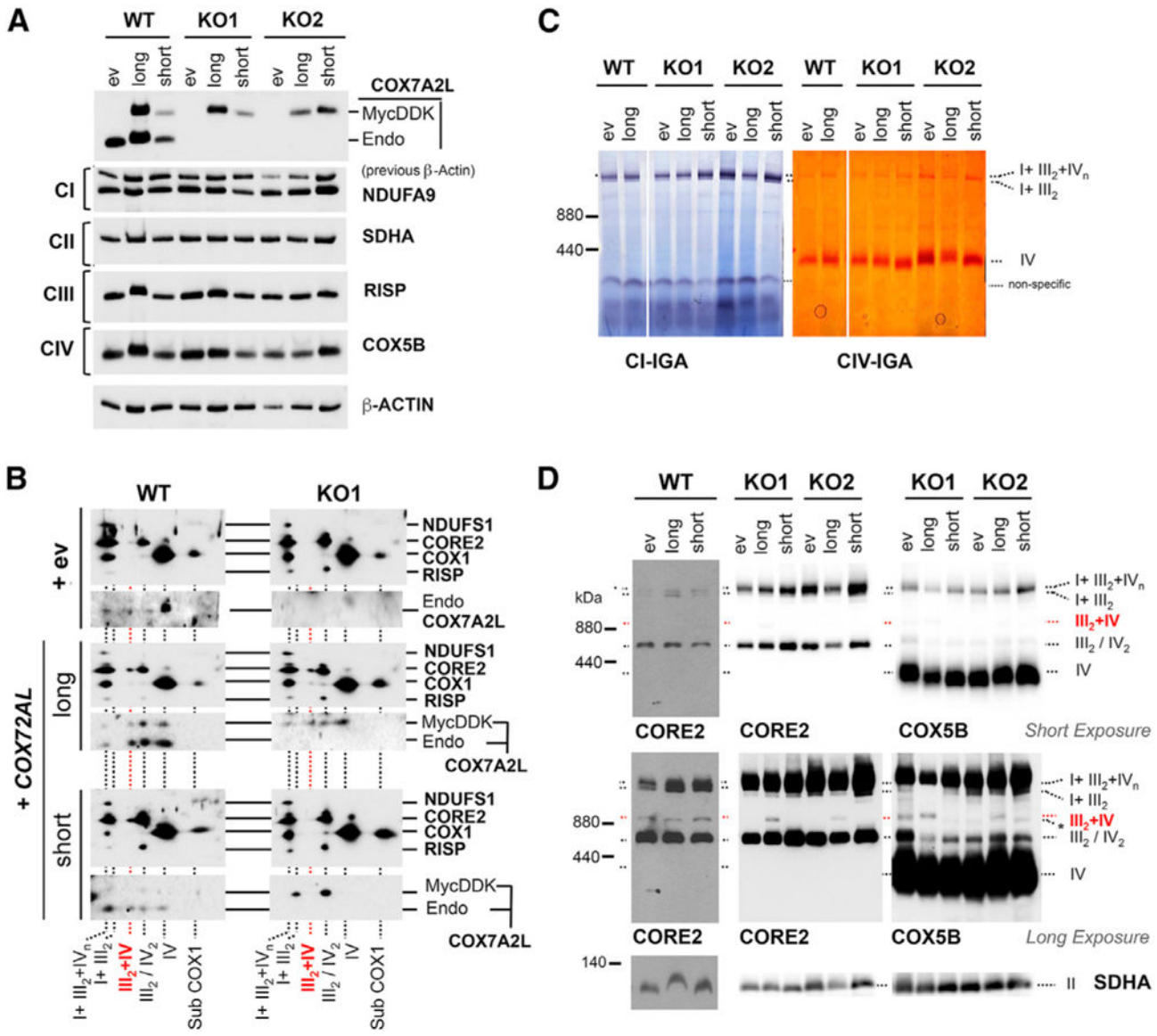

Figure 6. The Short-COX7A2L Variant Binds to CIII2 but Does Not Rescue SC III2+IV Assembly in COX7A2L-KO Cells

Control HEK293T cells (WT) and both *COX7A2L*- KO (KO1 and KO2) clones carrying an empty vector (ev) or constructs to overexpress COX7A2L-Myc- DDK (long) or short-COX7A2L-Myc-DDK (short) were used in the following experiments.

(A) SDS-PAGE followed by immunoblotting to estimate steady-state levels of endogenous COX7A2L (~12.6 kDa) from exogenous COX7A2L-Myc-DDK (~16.2 kDa). Membranes were also incubated with antibodies that recognize the indicated OXPHOS subunits.

(B). 2D-BN/SDS-PAGE and immunoblotting using digitonin-solubilized mitochondrial extracts (detergent/protein ratio, 4:1) and the indicated antibodies. (C and D) BN-PAGE followed by immunoblotting in digitonized whole-cell extracts (C) or by CI-IGA and CIV-IGA assays and/or immunoblotting in digitonized isolated mitochondria (D). Membranes were incubated with the indicated antibodies. I+III_2+IV_n, SCs containing CI, $CIII_2$, and CIV. I+III_2, SC containing CI and $CIII_2$. III_2+IV, SC containing $CIII_2$ and CIV. III_2, complex III

dimer ($CIII_2$). IV, complex IV; IV_2, complex IV dimer (CIV_2); II, complex II. Subcomplexes that contain COX1 are indicated as subCOX1. In (D), an unidentified band running a bit faster than the SC III_2+IV cross-reacting with the COX5B antibody (Ab) (but not with the CORE2 Ab) is indicated with an asterisk.

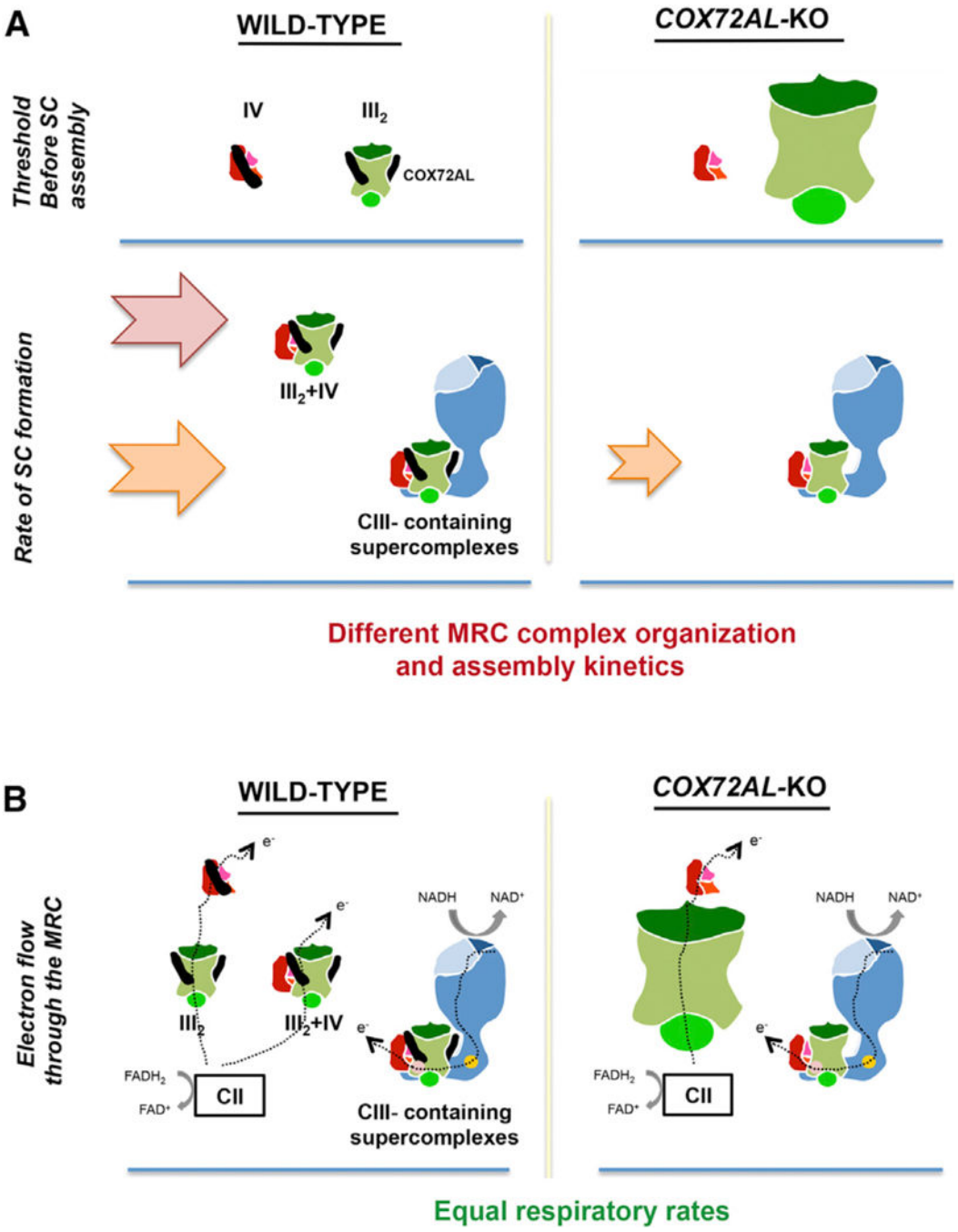

Figure 7. Structural and Functional Rearrangements of the RC in the Absence of COX7A2L

(A) Fully assembled $CIII_2$ and CIV accumulate until they reach a threshold that ignites SC III_2+IV and respirasome assembly at rates arbitrarily indicated by arrows. In the absence of COX7A2L, $CIII_2$ levels are ~2–3-fold, SC III_2+IV is not formed, and the assembly kinetics of CIII-containing SCs is slower.

(B) In physiological, nutritional, and environmental stress conditions, individual and simultaneous oxidation of NADH- and FAD-linked substrates is similar in WT and

COX7A2L-KO cells. Mitochondrial CI, $CIII_2$, and CIV are represented in blue, green, and red, respectively. COX7A2L is represented as a black stick.